The effect of long-term and decadal climate and hydrology variations on estuarine marsh dynamics: an identifying case study from the Río de la Plata

M. Schuerch[1], J. Scholten[2], S. Carretero[3], F. García-Rodríguez[4], K. Kumbier[5], M. Baechtiger[5], V. Liebetrau[6]

[1] University of Cambridge, Department of Geography, Cambridge Coastal Research Unit, Downing Place, Cambridge, CB2 EN3, United Kingdom

[2] Kiel University, Institute of Geosciences, Otto-Hahn Platz 1, 24098 Kiel, Germany

[3] Consejo Nacional de Investigaciones Científicas y Técnicas (CONICET), Facultad de Ciencias Naturales y Museo, Universidad Nacional de La Plata (UNLP), 64 no. 3, 1900 La Plata, Argentina

[4] Centro Universitario Regional Este, CURE-Rocha, Ruta 9 intersección Ruta 15, Rocha, Uruguay

[5] Kiel University, Institute of Geography, Ludewig-Meyn-Strasse 14, 24098 Kiel, Germany

[6] GEOMAR Helmholtz Centre for Ocean Research Kiel, Wischhofstrasse 1–3, 24148 Kiel, Germany

Corresponding address: Mark Schuerch, ms2358@cam.ac.uk, +44 1223 333192 (phone).

Abstract

The vertical growth of coastal wetlands is known to primarily be controlled by local tidal range and sediment availability as well as the occurrence of storm events. In estuaries, sediment availability additionally depends on riverine sediment input, the effect of which may be more pronounced in some parts of the estuary, thereby introducing a distinct spatial pattern that depends on the estuary's shape as well as the riverine sediment input and the hydro-meteorological regime.

In the present study, we investigate how estuarine marshes along the whole Río de la Plata (RdlP) are affected by decadal and long-term variations in river discharge and storm activity. The El Niño Southern Oscillation (ENSO), in this context, appears to introduce a pronounced decadal variability on sediment loads brought into the RdlP.

Based on 15 sediment cores, recovered along the RdlP and adjacent Atlantic coast, vertical marsh growth rates were studied using radionuclide dating (^{210}Pb and ^{137}Cs) and grain size distributions. By comparing these sedimentological records with historic river discharge and storm surge data, we spatially interpret the relative importance of temporal variations in river discharge and storm activity on estuarine marsh growth.

By delivering the first estimates for vertical growth rates of the RdlP marshes, we conclude that with average vertical marsh growth rates between 0.4 and 2.6 cm yr^{-1}, the RdlP marshes are highly resilient against drowning under present and future SLR conditions. Furthermore, our results confirm a large spatial variability of the drivers for vertical marsh growth; extreme storm surges appear to play a role in the development of the outer RdlP marshes whereas the temporal variations in river discharge seem to be hierarchically more important for the marshes in the inner estuary.

Keywords

Estuarine marshes, Río de la Plata, sediment deposition, decadal climate variability

1 Introduction

Estuarine marshes are increasingly recognized as important landscape features in the context of coastal management and coastal protection strategies (Shepard et al., 2011). Besides their high ecological value (Barbier et al., 2011), they are considered as a crucial element of the so-called ’building with nature‘ approach that seeks for alternative adaptation strategies to the classical hard defence structures in preventing flooding of populated coastal areas (Temmerman et al., 2013). Estuarine marshes were shown to efficiently dissipate wave and storm surge energy and decrease flood risks in coastal cities in the inner part of large estuaries (Temmerman et al., 2013; Bouma et al., 2014; Möller et al., 2014).

The morphological development of coastal (including estuarine) marshes strongly depends on the availability of suspended sediment, the local hydrological regime and wave climate as well as long-term SLR (van der Wal and Pye, 2004; Callaghan et al., 2010; Schuerch et al., 2013). In estuaries, the above-mentioned variables are controlled by the estuary's shape, river discharge, marine processes such as tides, waves, storm surges, and SLR, and interactions between these parameters (Dalrymple et al., 1992; Friedrichs et al., 1998; Uncles, 2002; Schuerch et al., 2014). Maximum suspended particulate matter (SPM), for instance, has been shown to increase with the length of the estuary and the prevailing tidal range as a consequence of increasing maximum tidal currents (Uncles et al., 2002). The tidal range within an estuary, in turn, strongly relies on the estuary's morphology, primarily the convergence and water depth. Tidal amplification is strongest observed in converging and deep estuaries, whereas the tidal wave is dampened in prismatic and shallow estuaries (Van Rijn, 2010). The estuary's shape also controls the wave exposure and associated sediment resuspension in the estuary. In response to these spatial patterns of the drivers for estuarine marsh morphology, spatial variations of both recent vertical growth through sediment accretion and lateral marsh dynamics within an estuary have been reported by various authors (Temmerman et al., 2004; van der Wal and Pye, 2004; Butzeck et al., 2014). Some stunning evidence for how sedimentation processes on marshes in a small river mouth system may be affected by decadal variations in the hydro-morphological regime has been presented by Clarke et al. (2014). Historical data, however, on how marshes respond to changes in the spatial patterns of the drivers for their morphological development, triggered by decadal and long-term variations of the hydro-meteorological and riverine regime, are lacking.

A small tidal range has been shown to significantly increase the contribution of storm events on long-term marsh growth to enhance the ability of coastal marshes to adapt to future SLR (Kolker et al., 2009; Kirwan et al., 2010; Schuerch et al., 2012) . This is due to the fact that storm activity induces larger wave heights and increases wave-induced sediment resuspension on the tidal flats adjacent to the coastal marshes. The increase in suspended sediment concentration (SSC) is proportionally higher in micro-tidal environments compared to macro-tidal environments (Kirwan and Guntenspergen, 2010). A larger tidal range, in contrast, enables sediment resuspension by tidal currents. The relative importance of current and wave-induced sediment resuspension strongly depends on the site-specific wave exposure and the prevailing current conditions (Fossati et al., 2014).

In estuarine systems, an additional source of suspended sediment is the riverine discharge, which is usually subject to considerable seasonal and inter-annual variations (Chen et al., 2006; Depetris, 2007). Most aquatic systems in South America are strongly affected by the El Niño Southern Oscillation (ENSO) in response to changes of rainfall patterns (Mechoso and Iribarren, 1992). Especially in the tropical regions of South-America both river and associated sediment discharge have been reported to strongly depend on ENSO (Restrepo and Kjerfve, 2000). Excessive rainfall events over south-eastern South America during warm ENSO years are responsible for increased river discharge into the Uruguay and Paraná rivers (Depetris et al., 1996; Bischoff et al., 2000; Grimm and Tedeschi, 2009; Barreiro, 2010), a signal that is also found in the geochemical composition of the RdlP sediments (García-Rodríguez et al., 2014).

Our study contributes to an improved understanding of the estuary-scale processes and their spatial variability affecting the morphological behaviour of estuarine marshes and control mechanisms of the decadal climate variability. We emphasize the spatio-temporal variability of estuarine marshes' sediment characteristics and vertical growth rates to relate these to estuarine gradients and historic hydrological data. As a case study, we investigate the freshwater, brackish, and salt marshes around the RdlP estuary (on the coasts of Argentina and Uruguay) (Fig. 1a), where the observed river discharge is highly dependent on ENSO (Depetris, 2007). More specifically, we (i) investigate the spatial variability of grain size and vertical marsh growth; (ii) assess the relative influence of riverine sediment discharge and marine drivers, namely the current and wave induced sediment resuspension, on the spatial grain size distribution and vertical growth rates; and (iii) analyse how decadal climate variations, e.g. triggered by ENSO, affect vertical growth rates and the ability of estuarine marshes to adapt to future SLR.

2 Methods

2.1 Study area

The RdlP is a funnel-shaped estuary with a length of about 280 km and a maximum width, at its mouth, of 230 km (Mianzan et al., 2001), which drains into the Atlantic Ocean at 35.5°S (Fig. 1). It is characterized by a micro-tidal regime (<1 m), with a higher tidal range along the Argentinean coast and a lower tidal range along the Uruguayan coast (Fig. 2).

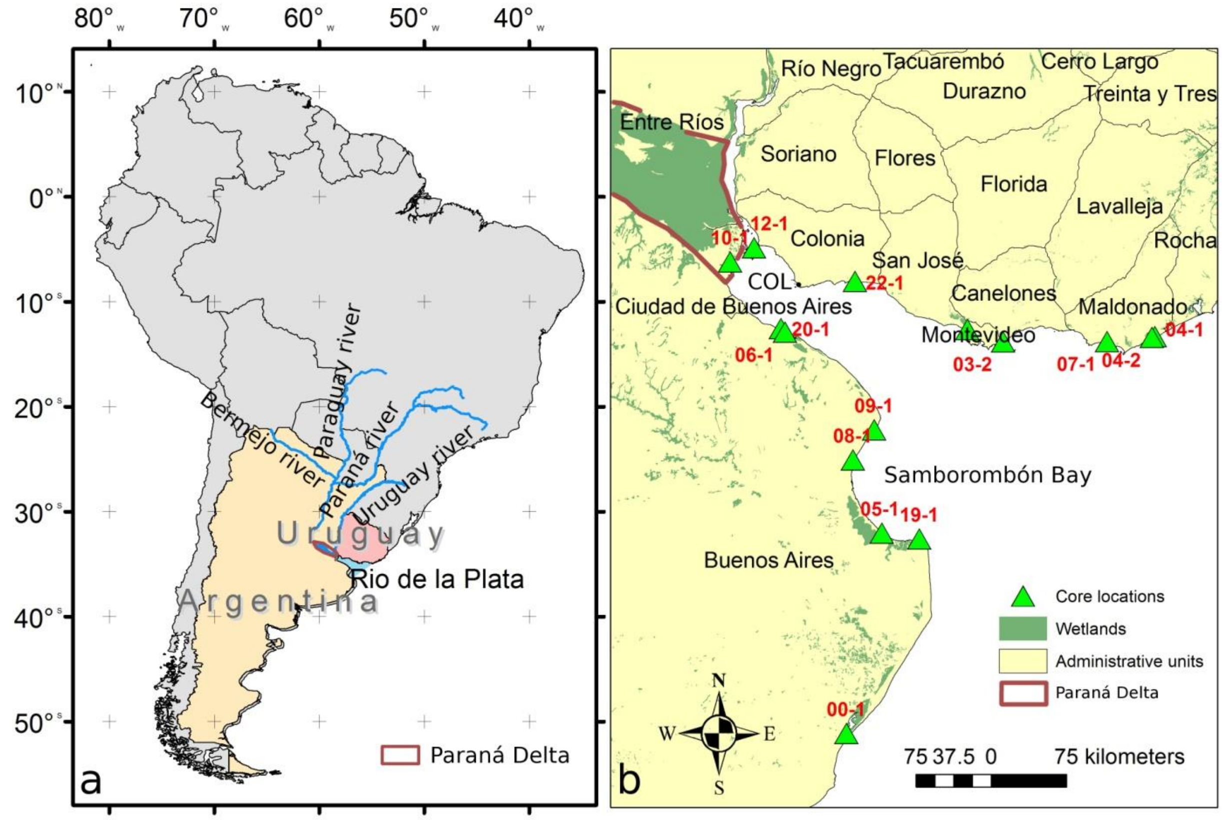

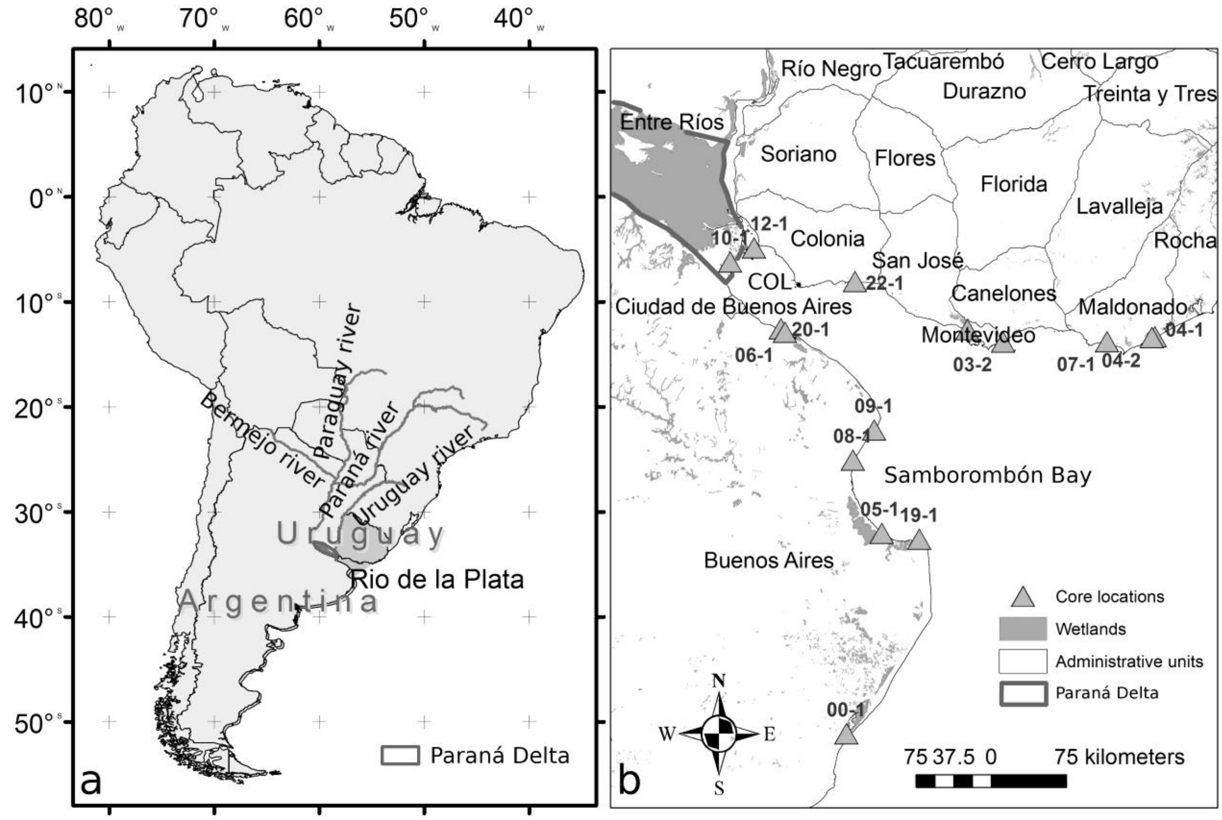

Figure 1: Location of the RdlP estuary (a) and the locations of the sampled estuarine marshes (b). For coordinates of the coring locations, see Table 1. COL: Colonia.

Formed at the confluence of the Paraná and the Uruguay rivers, the size of the RdlP drainage basin is 3.1 million km² (Acha et al., 2008). Annual mean river discharge into the RdlP amounts to ~20,000 m³ s^{-1} delivering ~79.8 billion kg of sediment yr^{-1}. SSC varies between 100 and 300 mg l^{-1} (Framiñan et al., 1999). Although intensive dam construction has taken place in the upper Paraná and Uruguay rivers during the 1970s and 1980s, river as well as sediment discharge has increased since the 1970s due to an increased proportion of sediment being delivered from the Bermejo River basin into the Paraná River (Amsler and Drago, 2009). Sediment loads in the Bermejo river have increased mainly due to more rainfall since the 1970s and due to the high erodibility of the mountainous catchment area (Amsler and Drago, 2009).

In the RdlP, a turbidity maximum zone (TMZ) forms in vicinity of the transition between the fresh, estuarine and the marine domain, depending on river discharge as well as the prevailing wind and tide conditions (Burchard and Baumert, 1998; North et al., 2004). The TMZ is generally characterized by a sharp decrease in SSC on the seaward side due to increased flocculation of fine-grained suspended sediments and, consequently, enhanced sediment deposition within the TMZ (Wolanski and Gibbs, 1995; Tatone et al., 2015).

The Paraná Delta is located in the innermost part of the RdlP (Fig. 1), adjacent to the city of Buenos Aires and has a size of about 14’000 km^2. It is prograding with a rate of up to 75 m yr^{-1} (Sarubbi et al., 2006). Seaward of the subaerial delta a subaqueous delta has formed, which extends about 200 km into the RdlP (Cavallotto et al., 2004) and is responsible for water depth of less than 10 m in most areas of the RdlP, including the Bay of Samborombón, where extensive salt marsh areas have developed (Fig. 1b).

2.2 Study sites

Our 15 study sites are situated along the Uruguayan and Argentinean coasts of the RdlP (Fig. 1b, Table 1). Locations of marsh cores were selected in the mid to high marsh zone (above the mean high water level), where a dense vegetation cover is present and inundation takes place irregularly. In these densely vegetated mid to high marshes, erosion can be neglected as the bed shear stress caused by currents and waves is extremely reduced by the vegetation (Fagherazzi et al., 2012). For two of the coring sites (08-1, 19-1), orthometric height measurements were conducted using GPS in kinematic mode (3 receptors Trimble model 4700 and 3 antennas Trimble model Microcentred L1/L2). The present marsh vegetation includes freshwater species in the inner estuary (e.g. *Ludwigia* spp., *Alternanthera philoxeroides, Echinodorus* sp., *Eryngium sp.*) and marine species (*Spartina densiflora, Juncus acutus*) in the outer estuary.

While the study sites along the Argentinean coast are located on the river banks of the RdlP (except for core 08-1 in the mouth of the Río Salado and core 00-1 in the lagoon of Mar Chiquita), the study sites along the Uruguayan coast (except cores 22-1 and 02-1) are located behind the sand barriers forming at the mouths of the small rivers draining into the RldP. All study sites, however, were chosen to be located in river mouths that are open all year round and as close to the inlet as possible.

2.3 Tidal range, wave exposure and suspended matter

For all 15 study sites tidal range, wave exposure and sediment availability were assessed by means of harmonic tides and GIS analysis, respectively. The amplitudes and periods of 12 tidal constituents (M2, S2, N2, K2, K1, O1, P1, Q1, M4, L2, S1 and Sa) were retrieved from the Simplified Empirical Tide Model (SEAT) (D'Onofrio et al.,

2012) for all 15 study sites and subsequently used to estimate the mean tidal range, based on a one-year tide prediction.

The assessment of site-specific wave exposure included the calculation of fetch lengths of all 15 study sites for 16 different wind directions, followed by both a bathymetry correction as suggested by Hill et al. (2010) and a correction for the prevailing wind conditions (Burrows et al., 2008). Uncorrected fetch lengths were limited to 250 km in order to account for wind-generated waves in the inner part of the estuary. Bathymetry data were retrieved from nautical charts, provided by the *Servicio de Hidrografía Naval, Argentina* (www.hidro.gob.ar/cartas/, 21.01.2013), whereas wind data (1979-2012) were gathered from the *NCEP-DOE* Reanalysis-2 project (http://www.esrl.noaa.gov/psd/data/gridded/, 30.01.2013). For those study sites that are located within a lagoon or behind a sandy barrier, site-specific wave exposure was assessed for the closest location along the coast that directly borders either the RdlP or the open sea. By doing this, we assume that marshes located within lagoons are supplied with sediment that has been resuspended along the open shore, rather than within the lagoon, where wave heights are negligible.

Average SSC (over 8 years) was calculated for every study site using SSC data that have been derived from MERIS satellite data for the RdlP region (Brockmann et al., 2012), obtained from www.coastcolour.org/site_27.html (07/03/2014). SSC data span from 2005 to 2012 with variable temporal resolution (between 22 and 191 datasets per year). We assume that the average derived from these data is a reliable estimate for the site-specific sediment availability.

2.4 Sample collection, grain size and C/N analysis

Fifteen marsh cores were obtained using PVC tubes with an inner diameter of 10.3 cm (Fig. 1, Table 1). Average core length was 79 cm with the longest core being 115 cm and the shortest core measuring 49 cm (Table 1). In the laboratory, the cores were sliced horizontally into 2 cm-layers between 0 and 20 cm of depth, 3 cm-layers between 20 and 50 cm, and 5 cm-layers below 50 cm of depth. X-ray images were obtained using a *Swissray ddR Multi System*, operated at 40 kV and 100 mAs and automatically controlled radiation time (Wetzel and Unverricht, 2013).

Core	Station Name	Longitude	Latitude	Length (cm)	Region within the estuary
00-1	Mar Chiquita	057°25.93' W	37°43.07' S	60	Southern Atlantic coast
19-1	Punta Rasa	056°46.71' W	36°19.29' S	106	Bay of Samborombón
08-1	Río Salado	057°22.38' W	35°44.73' S	115	Bay of Samborombón
05-1	Canal 1	057°06.90' W	36°16.72' S	73	Bay of Samborombón
09-1	Punta Piedras	057°11.01' W	35°31.47' S	112	Bay of Samborombón
20-1	Boca Cerrada	058°01.10' W	34°46.83' S	89	Middle estuary (Argentina)
06-1	Punta Lara	057°58.90' W	34°48.42' S	64	Middle estuary (Argentina)
10-1	Bajos del Temor	058°28.35' W	34°17.17' S	87	Paraná Delta
12-1	Isla Martín García	056°46.71' W	36°19.29' S	51	Paraná Delta
22-1	Boca Rosario	057°21.31' W	34°25.82' S	65	Middle estuary (Uruguay)
02-1	Santa Lucía	056°20.88' W	34°47.23' S	100	Middle estuary (Uruguay)
03-2	Arroyo Carrasco	056°01.66' W	34°52.68' S	72	Outer estuary (Uruguay)
07-1	Arroyo el Potrero	055°05.88' W	34°52.59' S	87	Northern Atlantic coast
04-1	José Ignacio	054°40.16' W	34°50.38' S	49	Northern Atlantic coast
04-2	José Ignacio	054°41.71' W	34°50.82' S	54	Northern Atlantic coast

Table 1: Core number, Station name, coordinates and length of all 15 cores extracted. Sorting of cores follows a virtual route from the southern Atlantic coast, into the estuary along the Argentinean coast (including the Bay of Samborombón), the Paraná Delta and back towards the Atlantic along the Uruguayan coast (Fig. 1).

All sediment samples were weighed before and after drying at 60°C until constant weight (>24 hours) in order to derive the dry bulk densities. Samples were then manually ground using mortar and pestle. Grain-size analysis was conducted with a *Malvern Mastersizer 2000* on aliquots of about 200-1000 mg after removal of the organic content (H_2O_2), potential traces of calcium carbonate (10% hydrochloric acid) and iron (sodium bicarbonate, sodium citrate, and sodium dithionate). Grain size data were analysed by comparing the complete frequency distributions as a function of depth as well as by analysing the grain size fractions sand (>63 µm), silt (<63 and >2 µm) and clay (<2 µm).

An element analyser *Euro EA* (gas chromatographer) was employed to assess the C/N contents of small representative aliquots of 25 ± 1 mg per sample. Inorganic carbon contents are assumed to be negligible, after minor reactions observed when adding hydrogen peroxide; hence, total carbon content (TC) is interpreted as a measure of the sample's organic carbon content.

2.5 Radionuclide analyses

For the age determination of marsh cores 02-1, 08-1, 10-1, 12-1, and 19-1 radionuclide analyses (excess ^{210}Pb and ^{137}Cs) were conducted by means of alpha- and/or gamma-spectrometry. Cores 02-1, 12-1, and 19-1 were analysed with alpha-spectrometry, whereas cores 10-1 and 08-1 were analysed with gamma-spectrometry. Compared to alpha-spectrometry the gamma method is less precise and has a higher detection limit, but allows for detection of the absolute ^{137}Cs marker horizon as an independent control on the ^{210}Pb-derived ages and the measurement of supported ^{210}Pb (via ^{226}Ra), which is needed to calculate excess ^{210}Pb activities. For cores where ^{210}Pb was determined by alpha-spectrometry selected samples were additionally measured by gamma-spectrometry to assess supported ^{210}Pb activities (via ^{226}Ra) and to determine the lowest depth where ^{137}Cs can be detected.

For alpha-spectrometric determination of ^{210}Pb ~300 mg sediment were digested in the presence of ^{209}Po yield tracer before polonium isotopes were counted using an *Ortec Octête Plus* alpha-spectrometer. The analyses were validated using *UREM-11* reference material. For gamma-spectrometric measurements two high-purity germanium detectors (*CANBERRA BE3830P*) were used to analyse ^{210}Pb, ^{226}Ra and

^{137}Cs for about 10-15 g of sediments. Unsupported ^{210}Pb ($^{210}Pb_{ex}$) was calculated as the difference between total ^{210}Pb and ^{226}Ra.

2.6 Dating model and derivation of deposition and accretion rates

The *Constant-Flux* (CF), also named the *Constant Rate of Supply* (CRS), dating model (Oldfield and Appleby, 1978; Appleby and Oldfield, 1983; Sanchez-Cabeza and Ruiz-Fernández, 2012) was applied to derive the year of deposition of a specific sediment layer from the unsupported ^{210}Pb activity measured in the samples. In cores that were too short to capture the total ^{210}Pb-inventory, necessary for the CF model, the *Constant Flux Constant Sedimentation* (CFCS) model was applied to estimate the missing inventory (Sanchez-Cabeza and Ruiz-Fernández, 2012). The marker horizon of known age, produced by the first deposition of ^{137}Cs in 1954 due to nuclear bomb testing, was used to validate the sediment ages derived from the CF model (Pennington et al., 1973; DeLaune et al., 1989).

Additional validation was conducted by means of LANDSAT satellite images from the years 1973, 1981, 1984, 1985, 1992, 1993, 2003 and 2013 (http://earthexplorer.usgs.gov/, 27.09.2013) that give information about historic land-building through lateral marsh expansion (Tosi et al., 2013). For study sites where marsh development has started after 1973 (first satellite image available) and the earliest measured date of sediment deposition in the respective core, a change in sediment characteristics is expected to be observed (e.g. transition from tidal flat to vegetated marsh). By comparing the CF-derived age of the sediment transition with the time period of land building, observed in the satellite images, an independent validation of the CF-derived sediment ages is possible (Schuerch et al., 2012).

Before vertical growth rates (cm yr^{-1}) were calculated from dating, the layer depths were corrected for sampling compaction as measured during core retrieval, assuming a linear compaction between the different measurements (4-5 per core). Thereafter, sediment deposition rates (kg m^{-2} yr^{-1}) were calculated as the product of the measured dry bulk density (kg m^{-3}) and the vertical growth rates.

2.7 River discharge

Data on monthly averaged river discharge of the two major rivers entering the RdlP (Paraná River and Uruguay River) were obtained from the *Integrated Hydrologic Database* from the *Secretariat of Water Resources, Argentina* (http://www.hidricosargentina.gov.ar/acceso_bd.php, 05.03.2014) as an indicative measure for the riverine sediment input that is to be closely related to river discharge (Amsler and Drago, 2009; Re et al., 2009). Discharge data (1909-2012) used for the Uruguay River were measured in Paso de los Libres, located about 600 km upstream, while data measured in the Paraná River (1905-2012) were obtained in the city of Paraná, located about 450 km upstream. Annual averages were calculated and subsequently smoothed using a moving-average filter with a window size of five years.

2.8 SEPI Index

Based on tide gauge data from Mar del Plata, located ~200 km south of the RdlP at the Atlantic coast, Fiore et al. (2009) developed an annual storm erosion potential index (SEPI), accounting for residual storm surge heights (above mean higher high water) and storm durations. Given that the storm intensity as well as the storm frequency have been shown to affect sediment accretion on coastal marshes (Schuerch et al., 2012), the SEPI index is assumed to well represent changes in the storm climate. Again, annual averages (1956-2005) were calculated, followed by smoothing using a moving-average filter with a window size of five years.

3 Results

3.1 Wave exposure, tidal range and SSC

Wave exposure (WE) is largest along the Atlantic coast outside the RdlP. However, the analysed marsh sites are not directly exposed to these wave conditions because they are located behind the sandy barriers forming at the river mouths, but they are assumed to be supplied with sediment that has been resuspended through wave action along the offshore barrier. Generally, WE within the inner RdlP is low, although variability is high. Highest WE indices within the inner RdlP are found at the sites 06-1 and 20-1, while lowest values are assessed in the Paraná Delta (cores 10-1, 12-1) (Fig. 2a). Meanwhile, highest tidal range (0.8-0.9 m) is observed in the Bay of Samborombón whereas lower tidal ranges (around 0.5 m) are determined towards the inner estuary. Along the outer Uruguayan coast tidal range is lowest (0.2 and 0.3 m) (Fig. 2b).

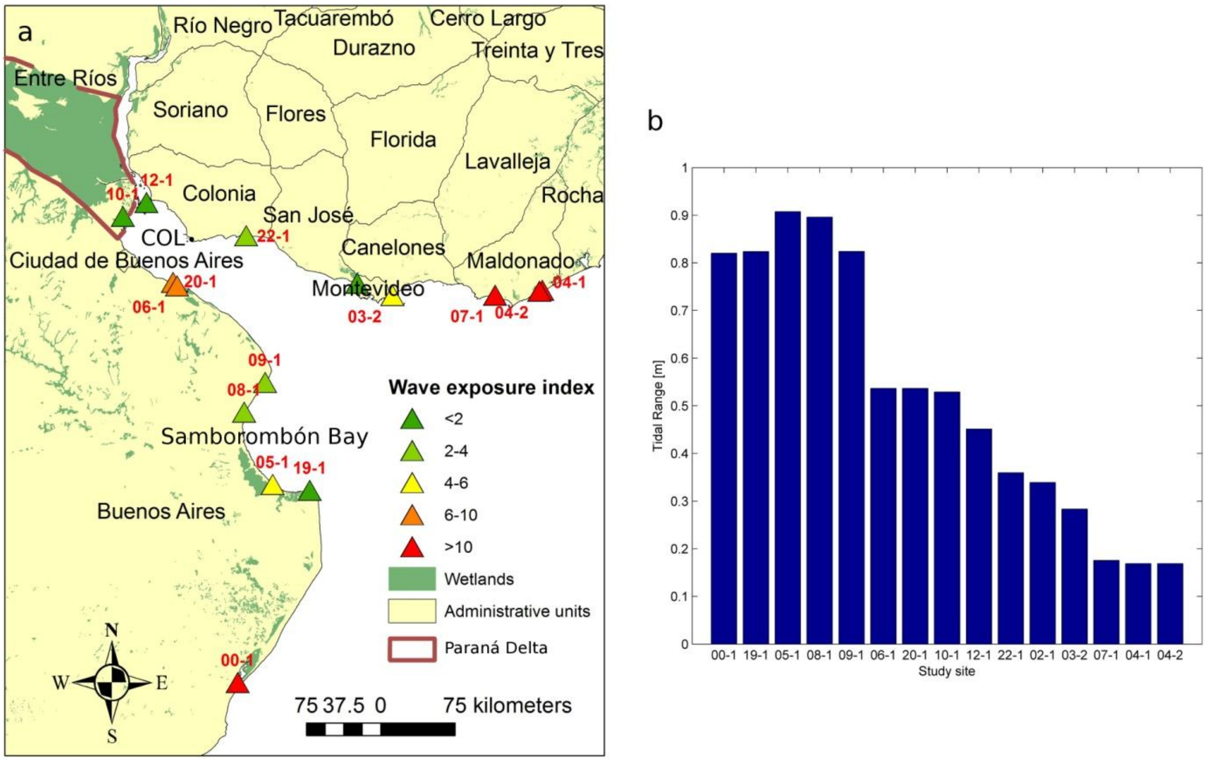

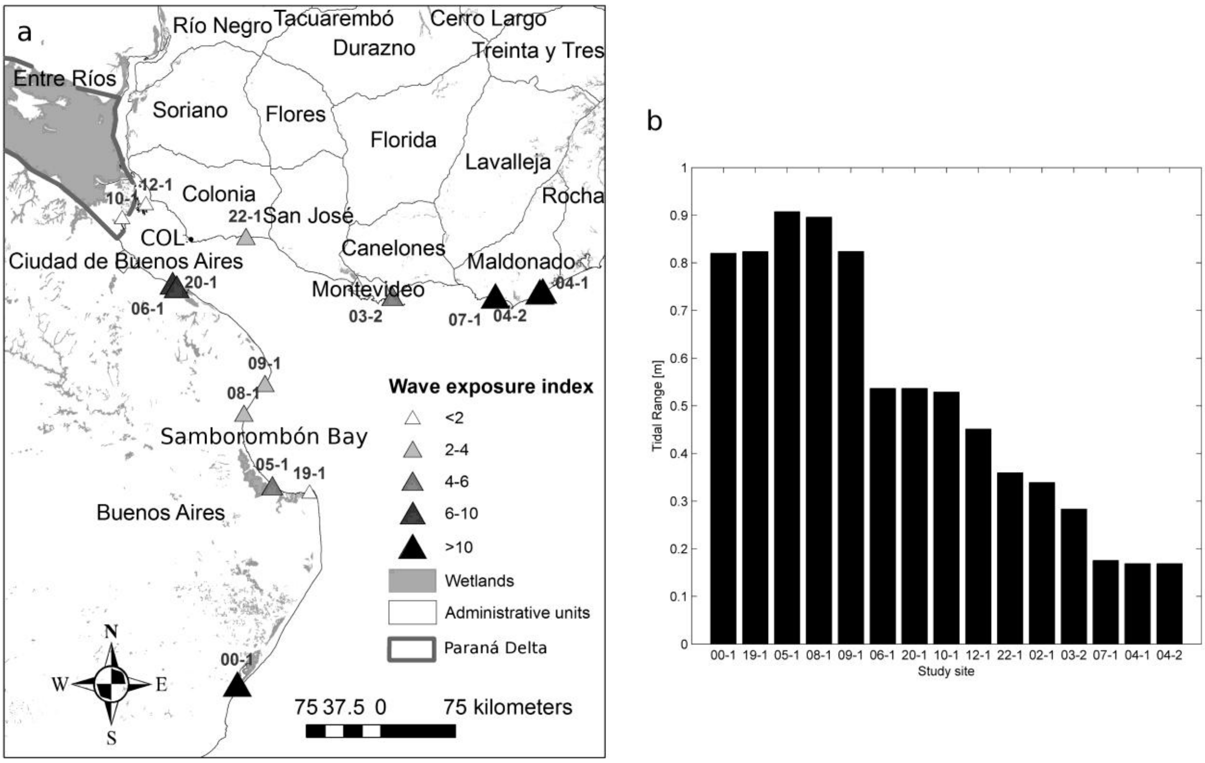

Figure 2: Calculated wave exposure (a) and tidal range (b) for all 15 study sites along the RdlP estuary.

As summarized in Table 2, the 8-year average (2005-2012) SSC is highest in the inner RdlP along the Argentinean coast and lower in the outer estuary and along the Uruguayan coast. Being a long-term average, these values are indicative for the average sediment availability integrating riverine and marine contributions for the different study sites. The temporal variability, represented by the standard deviation of the measured SSC time series, ranges between 23.5 and 57.4 mg l^{-1} and exceeds the average SSC in the outer part of the estuary where wave exposure is highest (Table 2).

Core	Average SSC (mg l^{-1})	Standard deviation	Region within the estuary
00-1	19.3	34.0	Southern Atlantic coast
19-1	51.9	23.6	Bay of Samborombón
08-1	92.3	37.2	Bay of Samborombón
05-1	67.4	24.4	Bay of Samborombón
09-1	140	57.5	Bay of Samborombón
20-1	143	43.3	Middle estuary (Argentina)
06-1	144	42.7	Middle estuary (Argentina)
10-1	126	40.1	Paraná Delta
12-1	117	42.0	Paraná Delta
22-1	109	36.6	Middle estuary (Uruguay)
02-1	54.8	37.5	Middle estuary (Uruguay)
03-2	26.5	28.2	Outer estuary (Uruguay)
07-1	21.9	41.6	Northern Atlantic coast
04-1	17.0	33.0	Northern Atlantic coast
04-2	16.7	32.3	Northern Atlantic coast

Table 2: Suspended sediment concentrations (average and standard deviation) determined for the 15 study sites and the regions as defined in table 1.

3.2 Grain size data

When analysing the grain size data of all cores, coarser sediments are generally recorded along the Uruguayan coast whereas finer sediments are observed along the Argentinean coast. In most cores an upward-fining trend is observed (Fig. 3). All sediment grain size distributions can be characterized by three modes that are found at the grain-size fractions 10-20 µm (mode 1), 160-200 µm (mode 2), and 500-1000 µm (mode 3). The cores 05-1 and 08-1 (Bay of Samborombón), 10-1 and 12-1 (Paraná Delta) as well as core 02-1 (West of Montevideo) show unimodal distributions with only mode 1 present. All other cores investigated show either a bimodal (cores 00-1, 19-1, 09-1, 20-1) or trimodal (cores 22-1, 03-1) distribution (Fig. 3). Mode 2 is most pronounced in the deeper parts of all bimodal and trimodal cores (dark lines in Fig. 3). With decreasing sediment depth, mode 2 appears to be reduced in favour of mode 1, whereas mode 3, only observed along the Uruguayan coast (cores 22-1, 03-1), is disappearing in favour of mode 2 (Fig. 3).

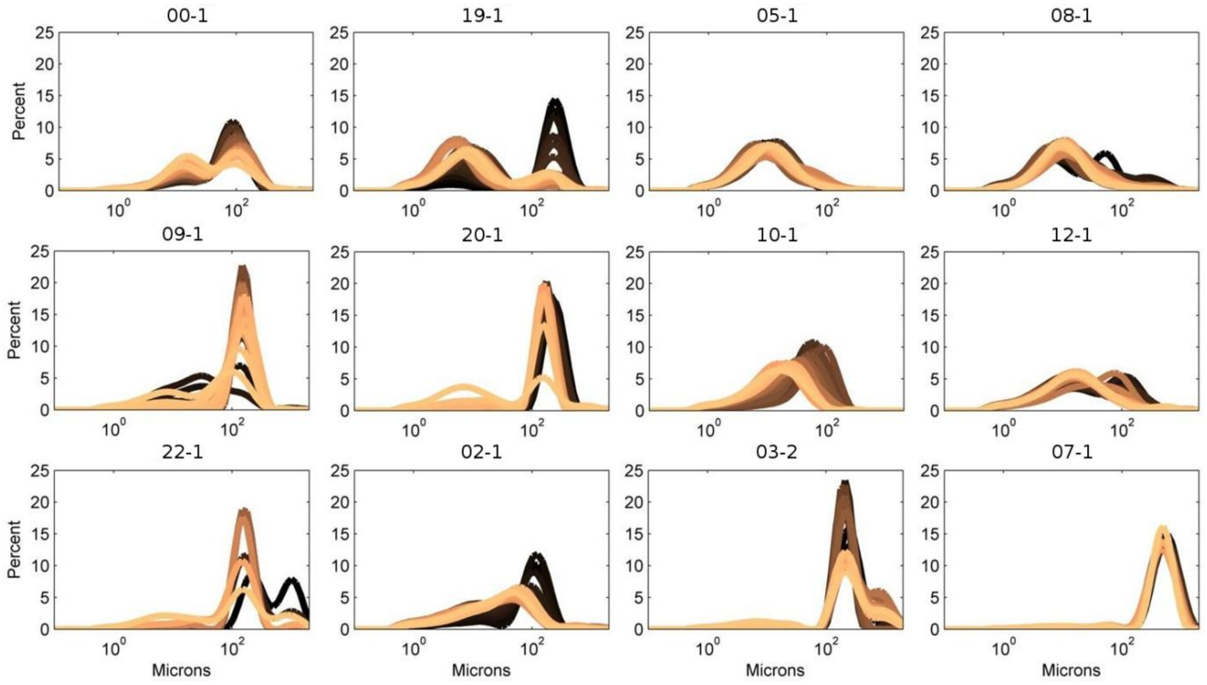

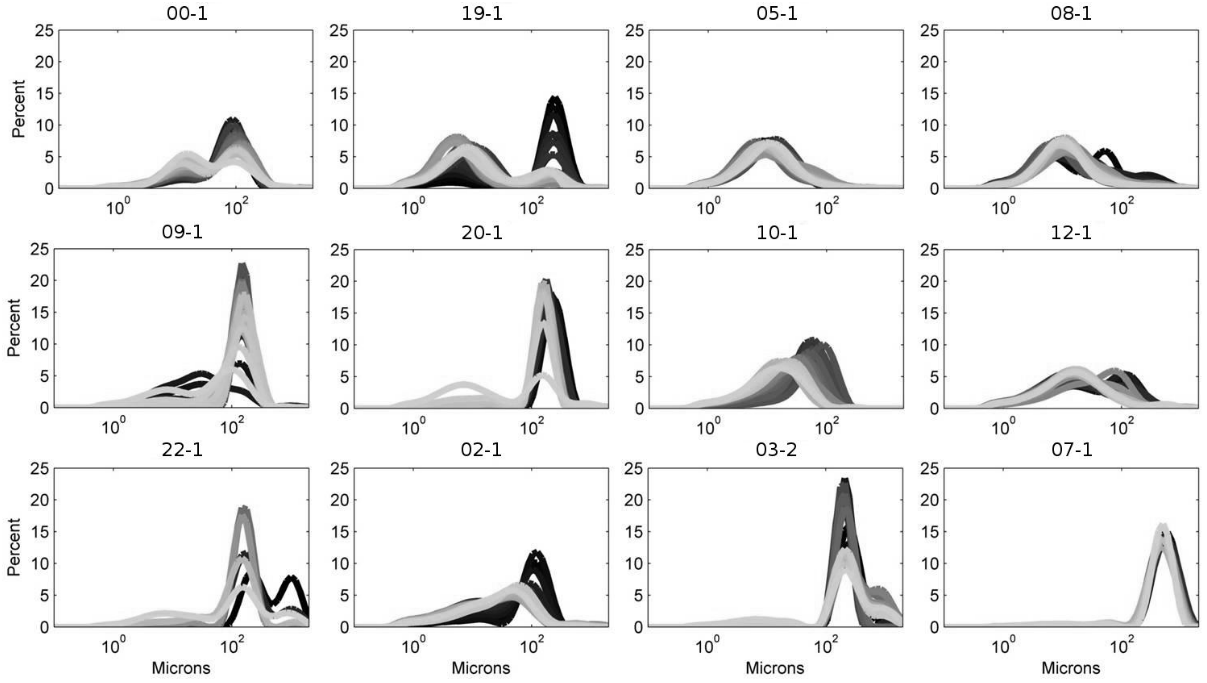

Figure 3: Grain-size distributions of the twelve most representative cores along the RdlP estuary. Dark colours indicate grain-size distributions of deeper layers, whereas lighter colours indicate shallower sediment depths. Note: The core lengths and, hence, the depth-indicating colours of the lines are not comparable between the cores.

The general upward-fining trend (Fig. 3) is also observed when looking at the changes in the grain-size fractions clay (<2 µm), silt (<63 µm) and sand (<2000 µm) (Fig. 4). From bottom to surface, a decrease in sand content is observed in cores 19-1, 10-1, 02-1, whereas this trend is less pronounced in the cores 08-1 and 12-1. Fig. 4 shows the ages of sediment layers derived from the CF-model (cores 19-1, 08-1, 12-1, 10-1, 02-1). We find that for the cores 19-1, 10-1, and 02-1 the observed fining trends are taking place in different time periods before the transition to the present constant grain sizes is observed in the late 1960s, early 1990s, and mid-1930s, respectively. Distinct layers of increased sand fractions are most pronounced in core 12-1 and tend not to be related to the occurrence of ENSO events (Fig. 4).

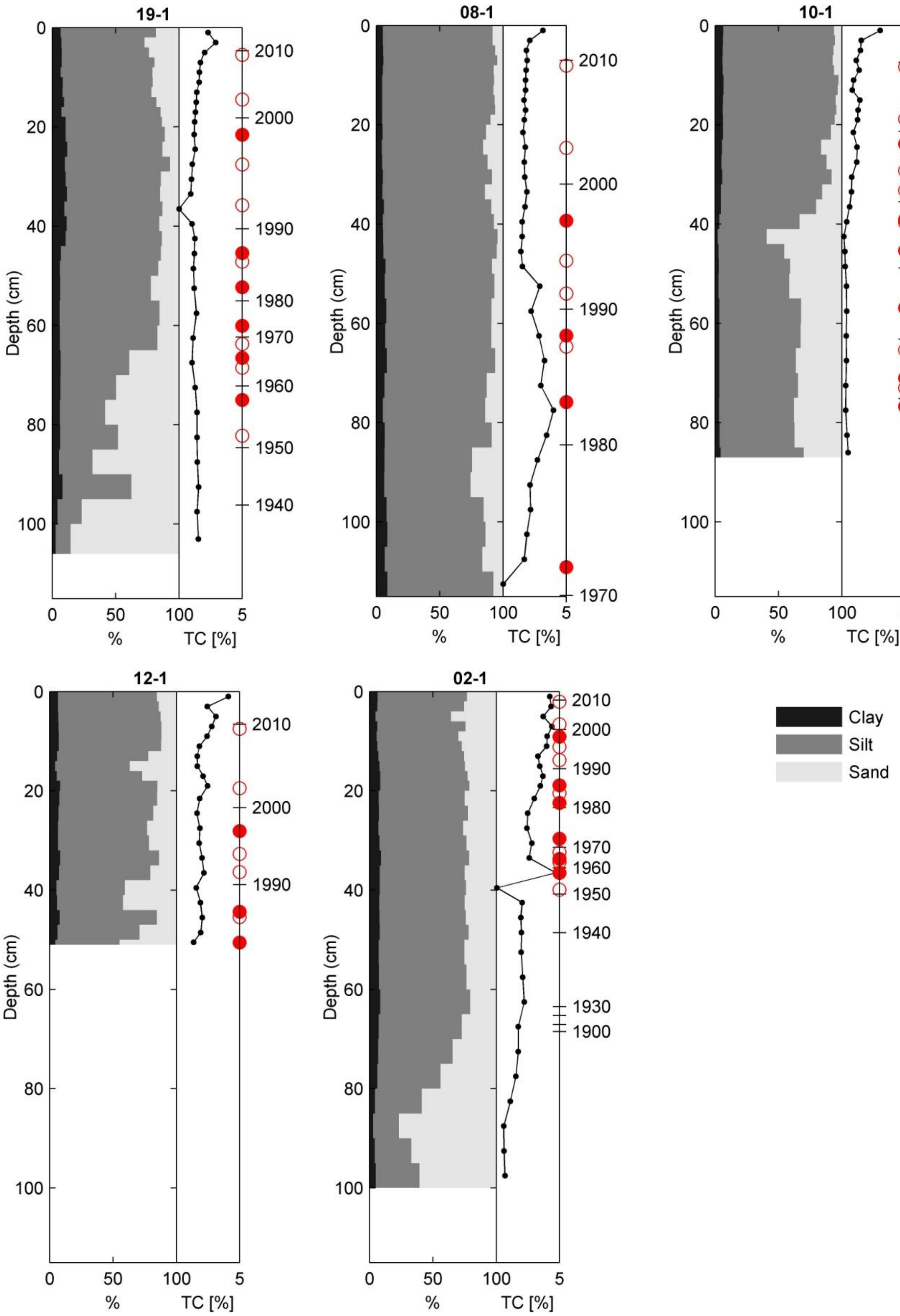
19-1
08-1
10-1
12-1
02-1
Depth (cm)
%
TC [%]
Clay
Silt
Sand

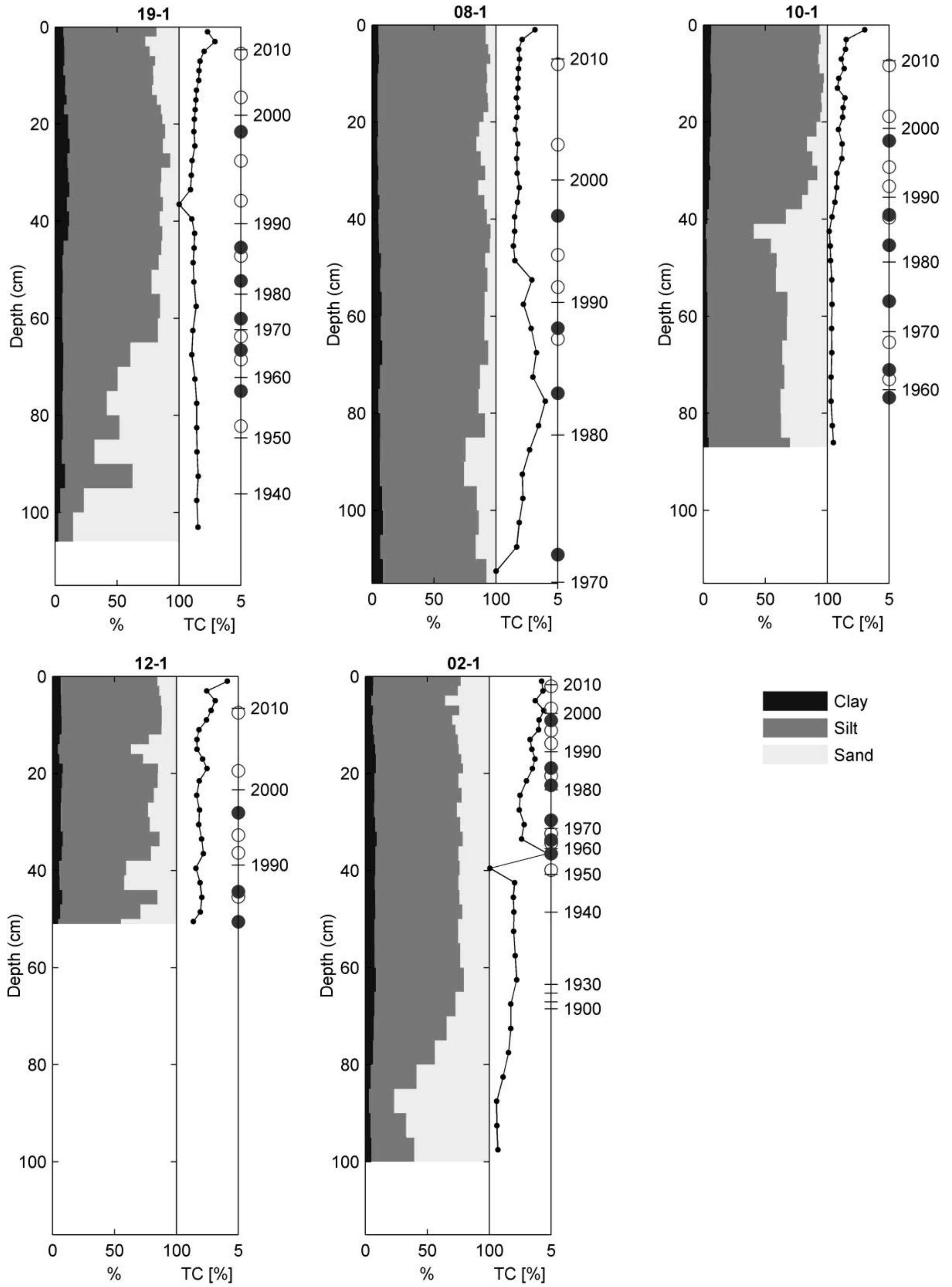

Figure 4: Grain-size fractions (sand, silt and clay, left panels) organic carbon content (≈TC, right panels) as a function of depth and time (resulting from ^{210}Pb dating presented in section 3.5, Fig. 6). Red filled dots indicate strong El Niño years; white dots indicate moderate El Niño events.

3.3 Organic carbon

The organic carbon (≈TC) content for all cores is <5% with the lowest values found in core 10-1, where TC is increasing in parallel to the silt and clay grain-size fractions (Fig. 4). In core 02-1 TC is independent of grain size, but higher in sediment depths <40 cm. In contrast, TC contents are lower in the upper layers (<50 cm) in core 08-1, whereas no significant changes are observed in cores 19-1 and 12-1 (Fig. 4).

3.4 X-ray radiographies

X-ray radiographies of cores 19-1, 08-1, 10-1, 12-1, and 02-1 allow identification of past depositional environment and the existence of (marsh) vegetation remains. Roots representing the existence of (marsh) vegetation are found throughout the cores 02-1, 08-1, and 12-1, whereas in core 19-1 the former sub-/intertidal environment can be detected at about 70 cm (very high abundance of mussel shells) (Fig. 5). In core 10-1, a clearly detectable shift from laminated/cross-bedded sub-/intertidal sediments to finer and less-structured marsh sediments is observed in about 40 cm of depth (Ta et al., 2002) (Fig. 5).

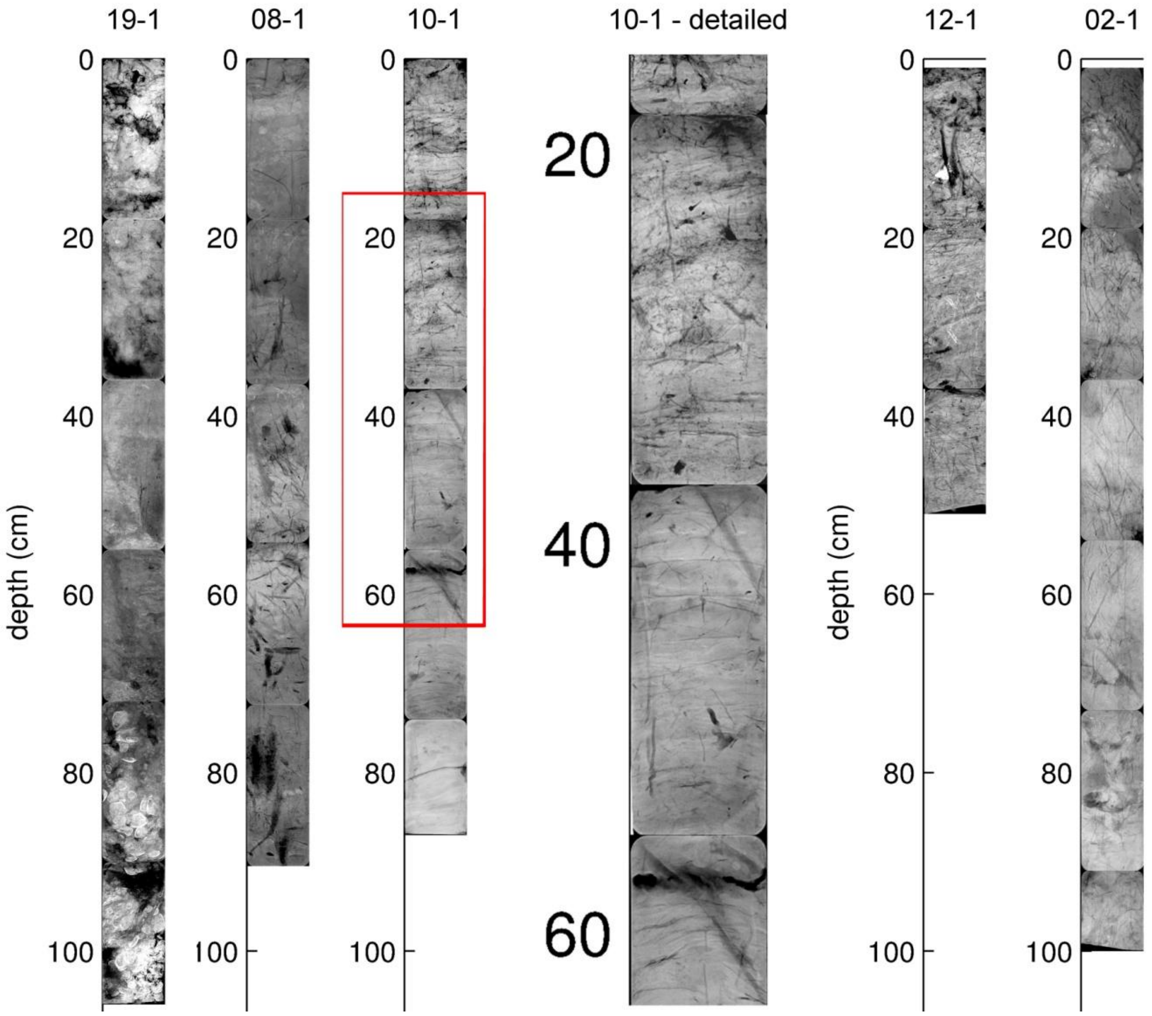
19-1
08-1
10-1
10-1 - detailed
12-1
02-1
depth (cm)
0
20
40
60
80
100

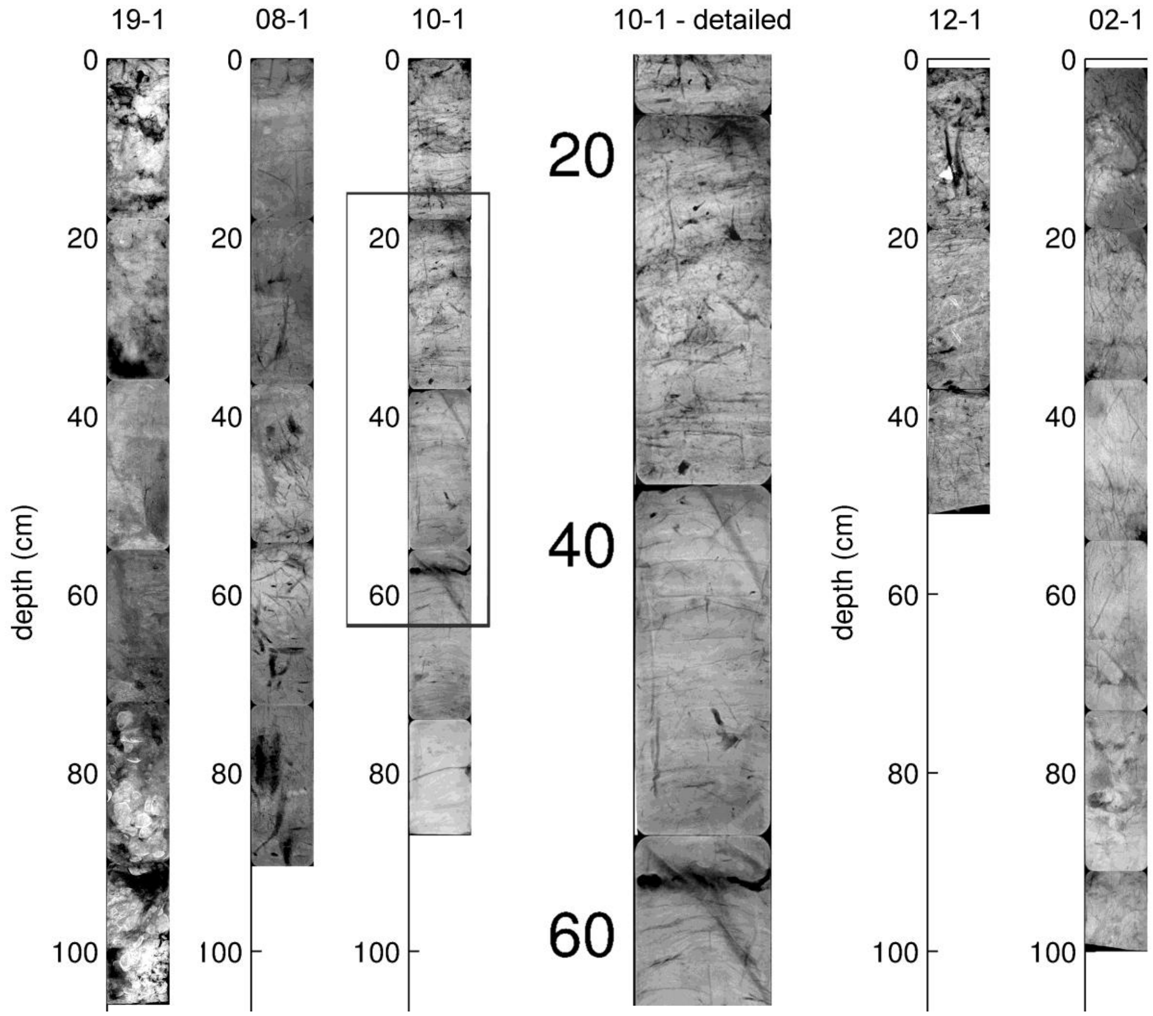

Figure 5: X-ray radiographies of the cores that have been dated by means of radioisotope analysis. Additionally, a detailed view on the transition zone from tidal flat to salt marsh in core 10-1 is shown in panel 4.

3.5 ^{210}Pb dating

The ^{210}Pb-derived sediment ages, calculated from the measured ^{210}Pb activities (see supplementary material) are displayed in Fig. 6. The measured historical marsh surface elevations considerably vary between the different study sites, with the fastest vertical growth (steepest curve) observed in core 08-1 and the slowest growth (flattest curve) in core 02-1. The length of the reconstructed time series goes back to the year 1858 in core 02-1, while only covering the time period after 1982 in core 12-1.

For all study sites the vertical marsh growth appears to lie well above the mean SLR measured during the past century in Buenos Aires (Holgate et al., 2012; PSMSL, 2015) (Fig. 6).

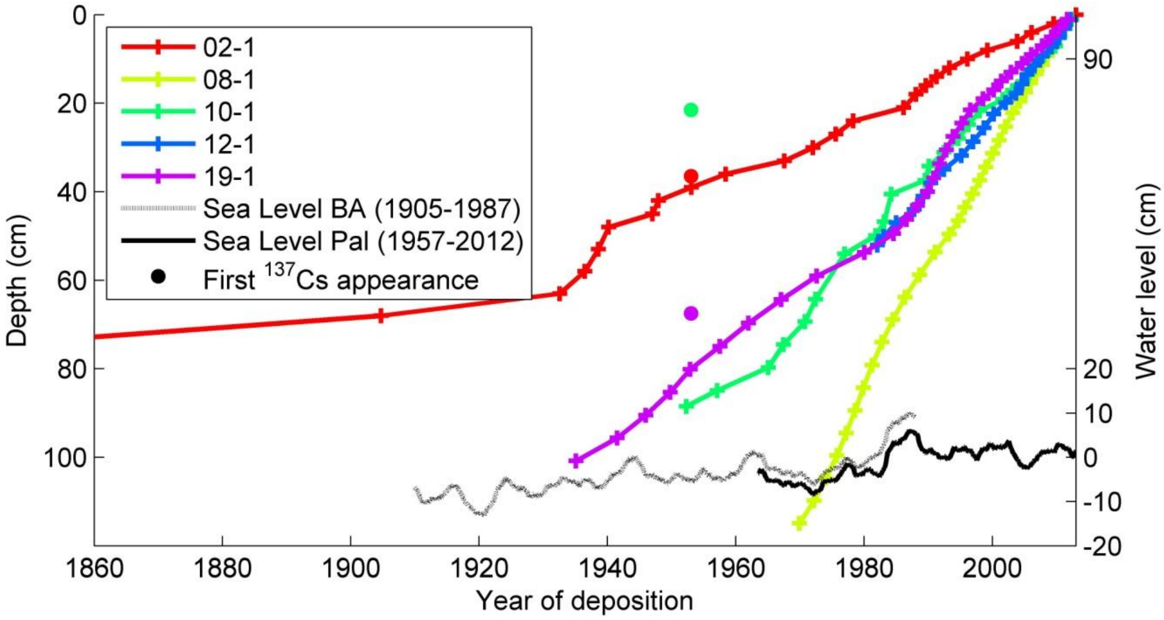

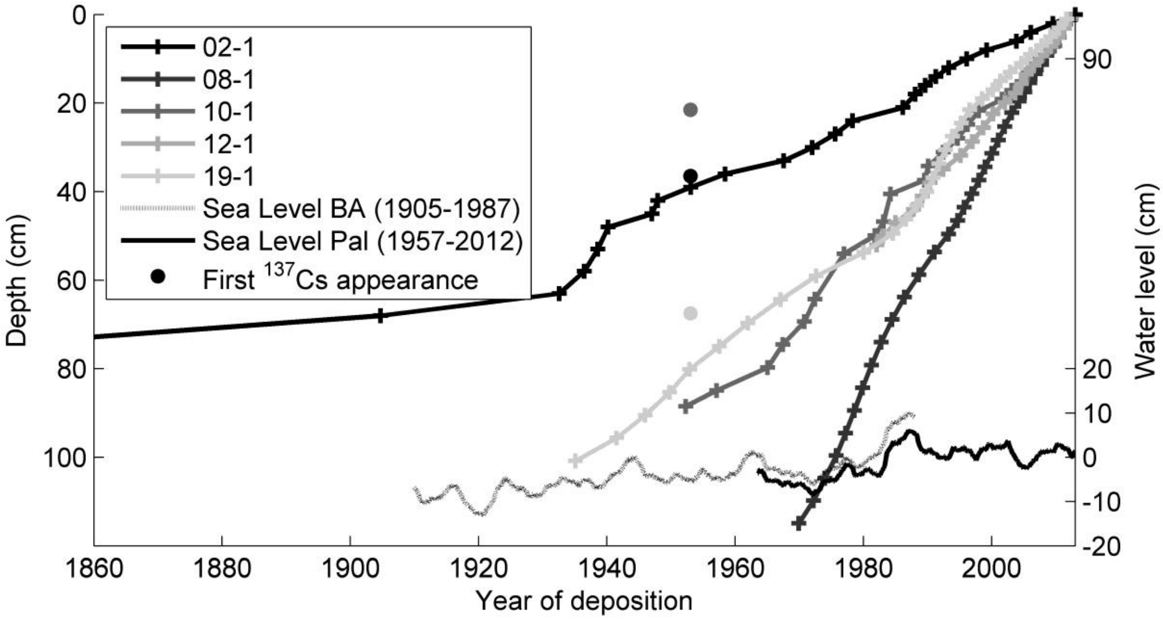

Figure 6: Age-depth curve for the different aged-dated cores (coloured lines). Coloured dots indicate the maximum depth of first appearance of ^{137}Cs. These dots are referred to as the year 1954, when ^{137}Cs was first released to the atmosphere. Where no dots are displayed ^{137}Cs was found throughout the whole core (see supplementary material). Dashed and solid black lines show the 5-year running mean of the monthly sea-level data for Buenos Aires (BA) and Palermo (Pal), respectively (Holgate et al., 2012; PSMSL, 2015).

Validation of the ^{210}Pb-derived sediment ages with the first occurrence of ^{137}Cs in 1954 shows a good agreement between both dating models. The best fit is observed for core 02-1. With exception of core 10-1, for which the assessed age could not be validated with the ^{137}Cs method, ^{137}Cs was found in all layers that are younger than 1954. In core 10-1, ^{137}Cs has been detected down to a depth of 24.5 cm only, whereas the CF-model indicates that sediments from 1954 correspond to a depth of about 87 cm (Fig. 6).

Meanwhile, the above described transition of a sub-/intertidal depositional regime to marsh sediments at 40 cm depth (Fig. 5) dates back to the year 1984, which is in close agreement with observations made in the LANDSAT images from 1981 to 1985, showing the beginning of land-building at the coring site as a consequence of rapid delta progradation by the middle 1980s (Fig. 7).

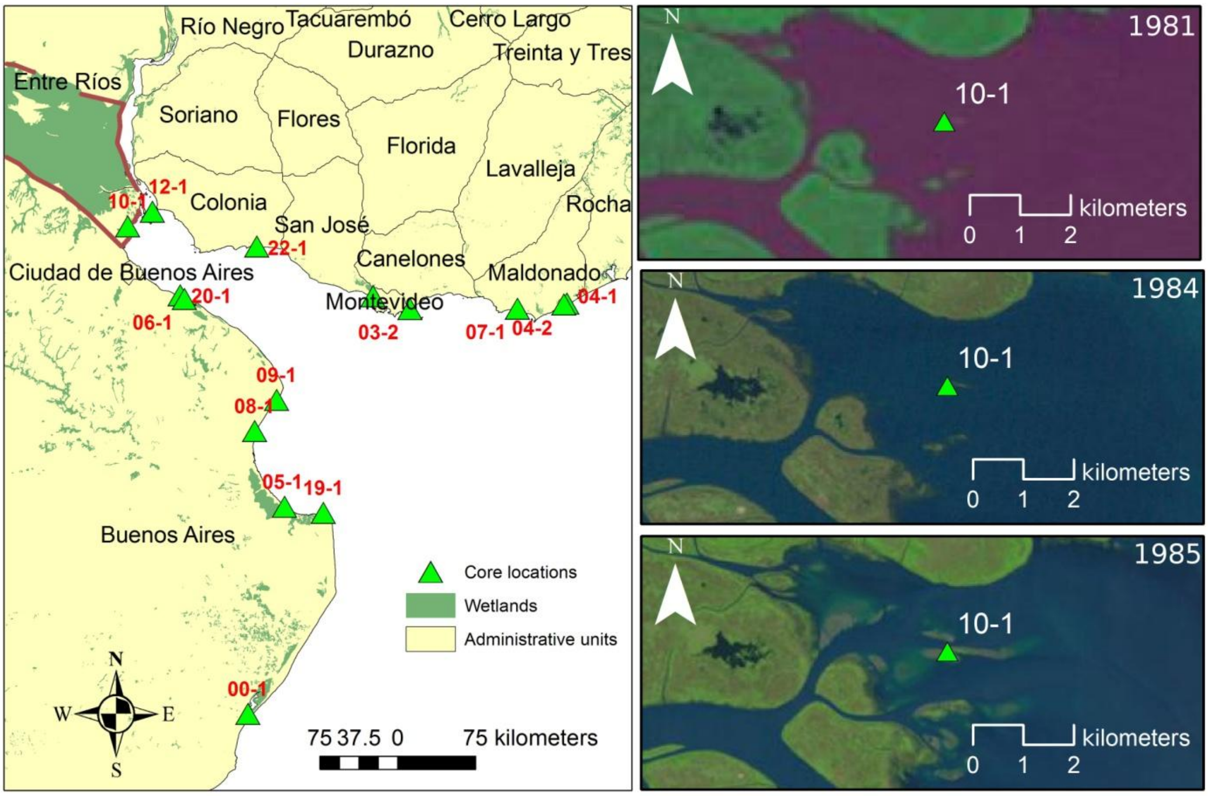

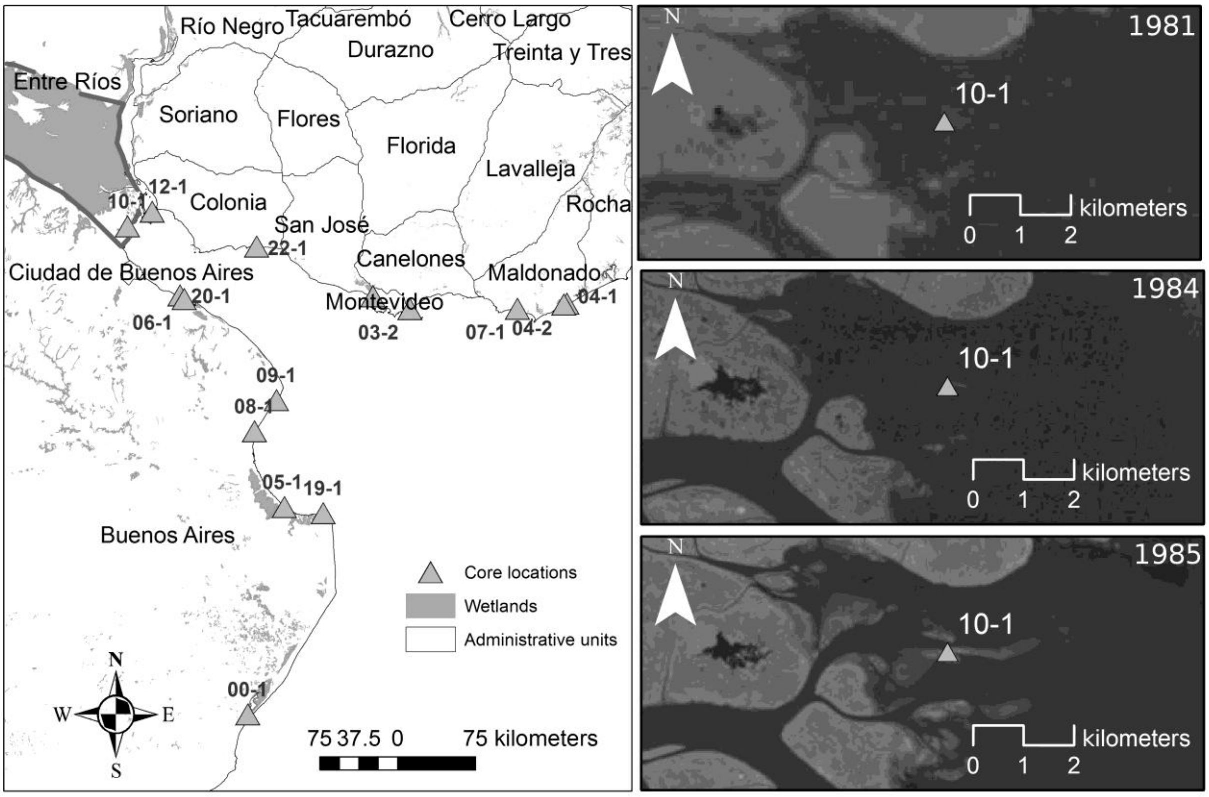

Figure 7: LANDSAT images (http://earthexplorer.usgs.gov/) for the surrounding of core 10-1 between 1981 and 1985, showing rapid delta progradation and land-building.

3.6 Site-specific vertical marsh growth

When comparing the vertical growth rates of the five dated cores a clear spatial pattern is detectable. Fastest marsh growth is observed in core 08-1 (Bay of Samborombón), whereas slowest growth is recorded for core 02-1 (Santa Lucía, Uruguay). Cores 10-1, 12-1 (Paraná delta), and 19-1 (Bay of Samborombón) are growing at similar rates (Table 3, Fig. 6). It should, however, be noted that direct comparisons of absolute growth rates between the different cores are of limited validity, since the exact elevations of the core locations are only known for the cores 08-1 and 19-1. Such comparison, however, indicates that core 08-1 shows considerably higher deposition and growth rates, although being elevated higher, than core 19-1 (Table 3).

Core	Average deposition rate (kg m^{-2} yr^{-1})	Average vertical growth rate (cm yr^{-1})	Orthometric height (m above MSL)
02-1	1.24	0.43	N/Á
08-1	9.15	2.62	1.71
10-1	8.60	1.52	N/Á
12-1	8.19	1.74	N/A
19-1	6.20	1.55	1.25

Table 3: Average deposition and surface elevation change derived from the CFCS dating model, together with the measured site elevation for the cores 08-1 and 19-1.

Considerable differences in temporal patterns of vertical growth rates between the five age-determined cores become apparent, when analysing the corresponding deposition rates (kg m^{-2} yr^{-1}) (Fig. 8). Recent deposition rates in the cores 19-1 and 10-1 tend to be higher than those observed prior to 1970; average pre-1970 deposition rates (5.61 kg m^{-2} yr^{-1}, 6.91 kg m^{-2} yr^{-1}) are lower than post-1970s rates (7.19 kg m^{-2} yr^{-1}, 9.98 kg m^{-2} yr^{-1}), although the two-sample t-tests cannot confirm significant differences ($p=0.16$, $p=0.09$). The opposite trend is observed for core 02-1 with an average pre-1970 deposition rate of 3.55 kg m^{-2} yr^{-1} and a post-1970s rate of 2.89 kg m^{-2} yr^{-1}, but no statistically significant difference was detected ($p=0.54$). Meanwhile, mean river discharge prior to 1970 (~16,900 m^3 s^{-1}) is significantly lower ($p<0.001$) than mean river discharge after 1970 (20,210 m^3 s^{-1}), whereas SEPI is not significantly different between the two periods ($p=0.77$) (Fig. 8).

Most of the depositional time series are characterized by distinct peaks that coincide with either the peaks in river discharge (Fig. 8a) or the storm surge index (SEPI) (Fig. 8b). Maximum deposition rates in cores 10-1 and 12-1, for example, are found in the years 1982 and 1983 during the historically most extreme El Niño event with the highest river discharge in records (Depetris, 2007). Peak deposition in core 19-1 is recorded in the year 1992, when river discharge is at its third highest peak level and the SEPI index is rapidly increasing. Similarly, the peak deposition during the recent decades has occurred in 1988 in core 02-1 (Fig. 8). No significant peaks but continuously high sediment deposition rates are observed in core 08-1 (in the inner Bay of Samborombón).

After the maximum peak deposition events in the early 1980s and 1990s, the temporal variability in deposition rates appears to be comparably higher in the cores of the inner estuary (cores 10-1 and 12-1), whereas deposition rates in the outer estuary (cores 08-1 and 19-1) as well as along the Uruguayan coast (core 02-1) appear to be relatively constant (Fig. 8).

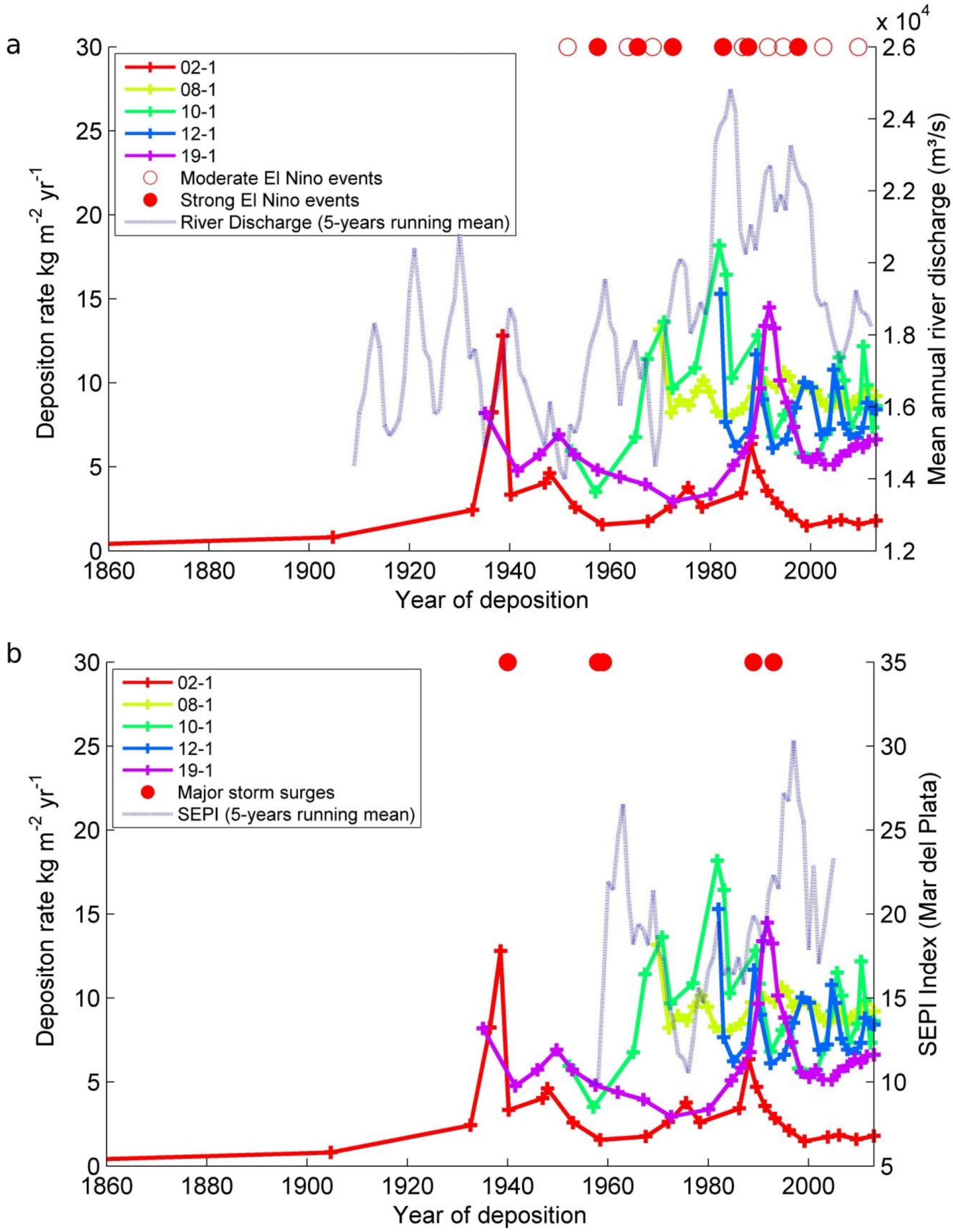
a
x 10^4
02-1
08-1
10-1
12-1
19-1
Moderate El Nino events
Strong El Nino events
River Discharge (5-years running mean)
Depositon rate kg m^-2 yr^-1
Mean annual river discharge (m³/s)
Year of deposition
b
02-1
08-1
10-1
12-1
19-1
Major storm surges
SEPI (5-years running mean)
Depositon rate kg m^-2 yr^-1
SEPI Index (Mar del Plata)
Year of deposition

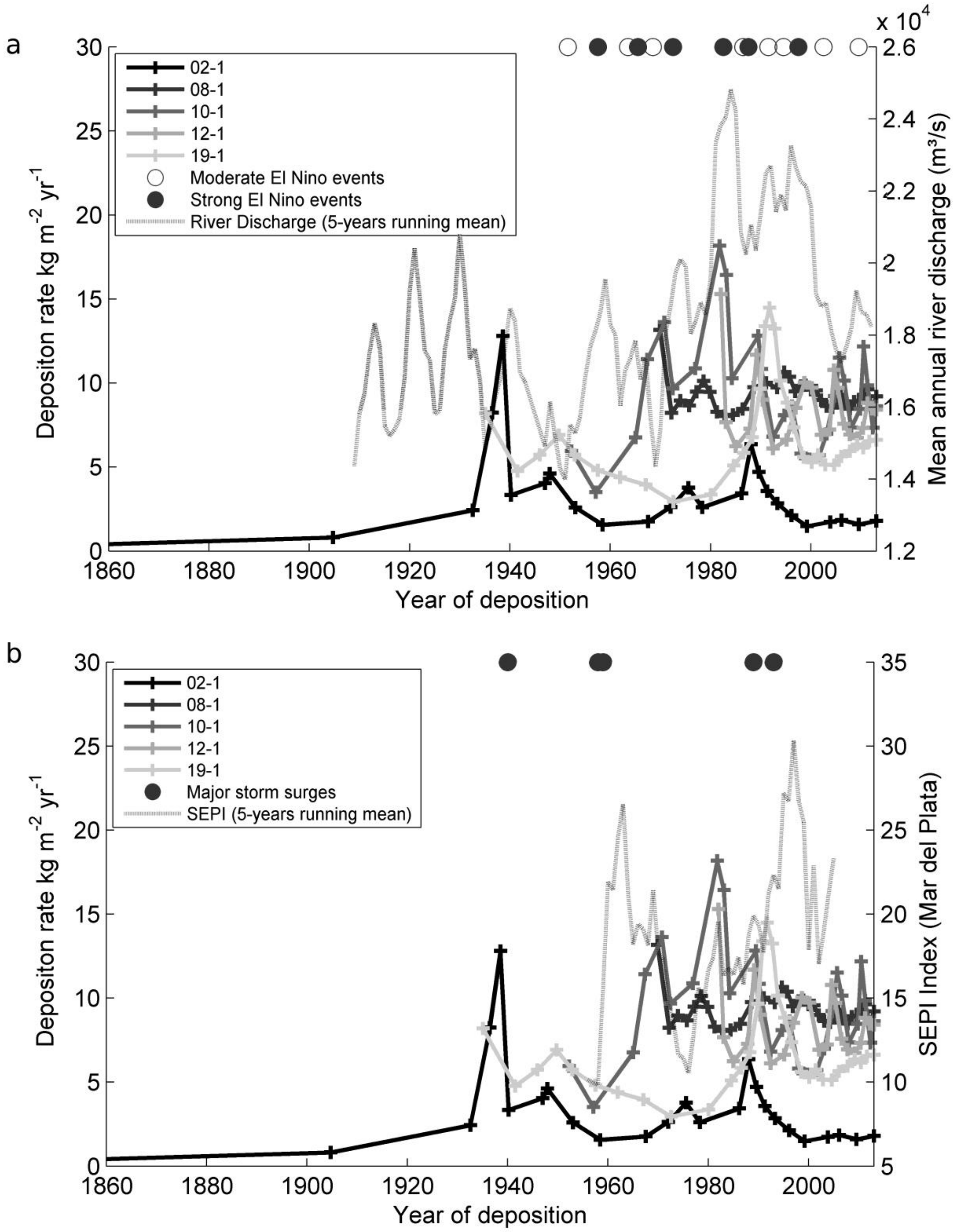

Figure 8: Changes in sediment deposition rates (kg m^{-2} yr^{-1}) for five selected cores around the RdlP estuary (solid lines) in comparison with the 5-year running mean river discharges controlled by the occurrence of strong (red filled dots) and moderate (white dots) El Niño events (a) and the SEPI-index together with the major storm surges in records following Isla et al. (2009) (b).

4 Discussion

4.1 Spatio-temporal variability of marsh growth in the context of estuarine sediment dynamics

4.1.1 Inner RdlP

The sediment transport and deposition processes in the RdlP are complex (Fossati et al., 2014). They are driven by marine (tides, waves, and storm surges) as well as terrestrial forcing (riverine freshwater and sediment inputs) (Laborde and Nagy, 1999). When entering the RdlP, riverine suspended sediments of the Paraná and Uruguay rivers are distributed according to their grain size. The coarser sediments are deposited in the Paraná Delta and its subaqueous elongation (Playa Honda); the finer sediments in the estuarine marshes and the outer RdlP (Menéndez et al., 2009).

Such a transition from fine to coarse sediments can also be observed in core 10-1, with fine sediments in the upper 40 cm and coarser sediments below (Fig. 4). The lower part of the core was likely formed before land-building had started around the mid-1980s as a consequence of the fast delta progradation (Fig. 7). The higher energy conditions on the previous tidal flat, compared to the presently vegetated marsh surface, promoted coarser grain sizes through bed load sediment transport. Today, the higher elevated estuarine marshes are exposed to lower energy conditions thus only allowing for suspended load transport of fined grained sediments (Rahman and Plater, 2014).

Throughout the whole core 12-1, in comparison, the distribution of fine-grained sediment fraction is rather constant (Fig. 4). Layers of clearly increased sand content around the years 1990 and 2005 are likely related to the occurrence of the historically most extreme storm surge events in 1989/1993 and 2005 (Isla et al., 2009). Deposition rates in these two time periods are also elevated due to the extreme storm events. Maximum deposition rates, however, for both “Delta cores” appear to be related to the period of maximum river discharge in 1982/83, triggered by one of the strongest recorded Niño events (Fig. 8a and b).

Overall, the delta marshes are growing much faster than MSL is currently rising (Fig. 6). Average SSC of the RdlP in its innermost part, where the Paraná Delta is located, is ~120 mg l^{-1} (cores 10-1, 12-1, Table 2), while exposure to waves is small (Fig. 2a). High sediment deposition rates in the forefront of the delta are responsible for the fast delta progradation between 50-75 m yr^{-1} in the southern part and 25 m yr^{-1} in the north (Menéndez et al., 2009) as well as for the high vertical marsh growth rates recorded for the “Delta cores”.

4.1.2 Middle RdlP

Fluvial freshwater discharge, sediment transport, and subaqueous channel erosion dominate the river bed morphodynamics in the middle part of the RdlP estuary between Colonia and Montevideo (Fig. 1b) (Laborde and Nagy, 1999). Measured grain-size distributions in the estuarine marshes of the middle estuary (cores 06-1, 20-1, 22-1) consequently appear to be dominated by coarser grain sizes around 160-200 µm (mode 2), with a general upward-fining tendency (Fig. 3). This trend may be associated with an increased proportion of suspended sediment load, resulting from the fast vertical marsh growth that exceeds local SLR (Rahman and Plater, 2014) (Fig. 6). While low-lying tidal flats and pioneer marshes are exposed to comparatively high wave action and current velocities, coastal marshes that are elevating relative to local MSL are exposed to reduced inundation depths and frequencies and get covered by a denser vegetation canopy up to an optimal inundation height (Morris et al., 2002). Direct wave impacts and associated bed load transport on the marsh surface are reduced due to the dissipation of hydrodynamic energy on the marsh platform (Möller, 2006; Möller et al., 2014). Similar upward-fining tendencies have been reported for salt marshes in the Dee estuary (UK) (Rahman and Plater, 2014).

The observed temporal variability of deposition rates in core 02-1, being considered representative for the middle part of the estuary neither seems to be directly driven by river discharge nor the SEPI index. Nevertheless, highest deposition rates over the past 50 years coincide with a period of most extreme storm surges (around 1990). In this region of the estuary high tidal currents as well as the occurrence of storm events have been shown to significantly increase SSC (Fossati et al., 2014), which, in turn, enhance marsh deposition rates (Kirwan et al., 2010; Schuerch et al., 2012). Interestingly, only the most extreme surge events (such as in 1989/1993) seem to have an effect on deposition rates.

4.1.3 Outer Uruguayan coast and Bay of Samborombón

Along the outer Uruguayan part of the estuary, sediment concentrations are comparatively low (core 03-1: 26.5 mg l^{-1}, core 07-1: 21.9 mg l^{-1}) and grain sizes in the marsh cores are sandy. While no upward-fining trend is observed for core 07-1, indicating low vertical growth rates in comparison to SLR (Rahman and Plater, 2014), a clear upward-fining trend is observed in core 03-1, which, however, could also be related to a significant change in the morphology of the sandy barrier (eastward migration) at the river mouth, where the core has been taken (Clarke et al., 2014).

The sediment dynamics in the Bay of Samborombón are characterized by a rapid decrease in SSC from the North (core 09-1: 140 mg l^{-1}) to the South (core 19-1: 51.9 mg l^{-1}). Due to an increased tidal range and higher tidal current velocities along the Argentinean coast (compared to the Uruguayan coast) fine-grained sediments are transported into the Bay of Samborombón, thus explaining the high SSC at the entrance of the Bay (Moreira et al., 2013). Meanwhile, a high residence time of 120 days, due to very small residual current velocities within the Bay of Samborombón, and the shallow water depths, which reduce hydrodynamic wave and current energy, facilitate enhanced deposition of fined-grained sediments (Piedra-Cueva and Fossati, 2007). Furthermore, the Bay of Samborombón is located where a well-mixed freshwater/salt water boundary and associated TMZ is developing, the exact location of which depends on the prevailing wind forcing and river discharge (Framiñan et al., 1999; Laborde and Nagy, 1999). The very fine-grained sediments transported into the Bay of Samborombón can settle only due to increased sediment flocculation within the TMZ (Framiñan and Brown, 1996).

The performed grain-size measurements confirm the dominance of very fine sediments in this area (cores 05-1 and 08-1) throughout the whole cores (Figs. 4, 5). Although the vertical growth rate of core 08-1 is the highest for the whole estuary, no upward-fining trend is observed and no layers of increased grain-size are found since the suspended sediment in the Bay of Samborombón likely does not contain any substantial coarse-grained sediment. The measured deposition rates are very high and remarkably constant throughout the whole core. A possible reason for this low variability could be the high water residence time within the Bay of Samborombón (Piedra-Cueva and Fossati, 2007). Interestingly, no changes in sediment composition and deposition rates are detected, before and after the dredging of drainage channels in 1987 and 1996 for the Río Salado at the mouth of which core 08-1 is located (Tosi et al., 2013). This implies that the sediment deposited there is primarily originating from the RdlP rather than supplied by the Río Salado.

4.2 Marsh growth data in the context of previous morphodynamic assessments

Our data on grain-size characteristics and vertical marsh growth is the first attempt to use the sediments from estuarine marshes of the Río de la Plata as archives to derive information on estuarine morphodynamics and associated estuarine marsh development. It represents the first dataset for RdlP marshes describing their historic development and addressing the question of how resilient these estuarine marshes are to climate change. Possibilities of direct comparison of our data to previous assessments are, therefore, limited. Recent vertical growth rates of 2.7 cm yr^{-1}, derived from ^{210}Pb measurements (Bonachea et al., 2010), as well as vertical accretion rates of 5 cm yr^{-1}, derived from sediment traps (Colombo et al., 2005), both measured on the tidal flats in vicinity of our cores 08-1 and 20-1, respectively (see Fig. 1b, Table 1), confirm the order of magnitude of the vertical growth rates presented within this study.

Although only three out of five of our marsh cores date back to prior to 1970, we observed a tendency of increased marsh deposition as well as vertical marsh growth rates after 1970 in the inner RdlP (10-1) and the Bay of Samborombón (19-1). Such an increase has previously been observed by Bonachea et al. (2010) in tidal flat growth rates, and is accompanied with a significant increase in precipitation over south-eastern South America and in river discharge (García and Vargas, 1998; Berbery et al., 2006; Marrero et al., 2014). While prior to 1970, marsh deposition rates seem not to respond to changes in river discharge and storm surge activity, after 1970, the frequent occurrence of high river discharge due to several significant ENSO events (e.g. 1982/83) as well the occurrence of extreme storm surge events appears to have a larger impact on marsh deposition. Given the limited vertical resolution of the employed dataset, we cannot certainly conclude on whether it is only the most extreme ENSO and storm surge events that influence that marsh deposition rates or whether smaller events could also have a significant effect. For microtidal systems, however, it is known that extreme events are relatively more important for marsh deposition than for macrotidal systems (Cahoon, 2006; Kolker et al., 2009).

Our data consistently indicate very high deposition rates, enabling the RdlP marshes to vertically grow fast enough to cope with present and, most likely with future SLR all around the RdlP (Fig. 7). This is especially relevant for the lowlands/salt marshes in the Bay of Samborombón that is one of the most important agricultural regions of Argentina (Jelgersma et al., 2002), and that is designated as a wetland of international importance (i.e., RAMSAR site). Tosi et al., (2013) assume a substantial coastline retreat of up to 40 km under the highest SLR scenario (120 cm until 2100) due to submersion under a scenario of no increase in the marsh elevation. Our data suggest, however, that flood risks may in fact be reduced along the Bay of Samborombón even under high SLR projections (Vermeer and Rahmstorf, 2009; Church et al., 2013).

4.3 Implications for estimation of the future development of estuarine marshes

The future development of coastal marshes was previously shown to be significantly affected by changes of the tidal range (Kirwan and Guntenspergen, 2010), the intensity and frequency of storm surges (Schuerch et al., 2013) as well as the prevailing wave climate (van der Wal and Pye, 2004). For the estuarine marshes in the RdlP we show, however, that river discharge as an additional driver, including its temporal variability, also has to be considered for estimating future marsh development and the marshes’ ability to adapt to future SLR. Moreover, the relative importance of this driver varies spatially within the estuary and depends on the location within the estuary. The difference observed between the Argentinean and Uruguayan side of the RdlP is a result of the differential site-specific tidal dynamics within the estuary, whereas the difference observed the inner and outer estuary is likely to be representative for many other large estuaries.

5 Conclusions

We present for the first time marsh deposition as well as vertical growth rates for estuarine marshes along the RdlP. By comparing the distinct rates of five representative study sites along the estuary, we contribute to a better understanding of estuarine sediment transport and deposition processes. Vertical marsh growth within the inner estuary and along the Argentinean coast is considerably higher than along the Uruguayan coast where sediment availability is lower (Table 2). Furthermore, the data show that vertical growth rates are substantially higher than the current and expected future SLR rates; hence, RdlP marshes are likely to adapt to future SLR.

After analysing the spatial pattern of grain-size distributions and vertical marsh growth rates, we infer that the riverine sediment discharge is the major driver controlling sediment delivery in the inner of the estuary, whereas in the outer estuary the importance of storm surge activity is enhanced. Storm surges, however, need to be of extreme nature to effectively increase marsh deposition rates. Consequently, the marsh deposition rates were found to be subject to increased temporal variability in the inner estuary compared to a lower variability that was observed in the salt marshes of the outer estuary.

Based on our results, we conclude that the morphodynamics of the freshwater marshes in the inner estuary are strongly affected by riverine sediment discharge that often is controlled by decadal climate variability (e.g. ENSO). Salt marshes in the outer estuary are more impacted by marine drivers, such as storm surges that may as well be subject to decadal variations.

Acknowledgment

This project (CP1211) was financially supported by a grant of the Cluster of Excellence 80 ‘The Future Ocean’ to Mark Schuerch. ‘The Future Ocean’ is funded within the framework of the Excellence Initiative by the ‘Deutsche Forschungsgemeinschaft’ (DFG) on behalf of the German federal and state governments.

Felipe García-Rodríguez acknowledges ‘Agencia Nacional de Investigación e Innovación’ (ANII). Jan Scholten acknowledges the support provided by the FP7 EU Marie Curie Career Integration Grant (grant PCIG09-GA-2011-293499).

Additionally, we like to thank our recently deceased colleague and friend Enrique Schnack for inspiring discussions as well as María Eugenia Gómez and Santiago Perdomo from the Faculty for Astronomical Sciences and Geophysics of the University of La Plata (Argentina) for their help in measuring the marsh elevations of the cores 08-1 and 19-1 and the two anonymous reviewers for their valuable comments.

References

Acha, M.E., Mianzan, H., Guerrero, R., Carreto, J., Giberto, D., Montoya, N. and Carignan, M., 2008. An overview of physical and ecological processes in the Rio de la Plata Estuary. Cont. Shelf Res., 28(13), 1579-1588.

Amsler, M.L. and Drago, E.C., 2009. A review of the suspended sediment budget at the confluence of the Paraná and Paraguay Rivers. Hydrol. Processes, 23(22), 3230-3235.

Appleby, P.G. and Oldfield, F., 1983. The assessment of 210Pb data from sites with varying sediment accumulation rates. Hydrobiologia, 103(1), 29-35.

Barbier, E.B., Hacker, S.D., Kennedy, C., Koch, E.W., Stier, A.C. and Silliman, B.R., 2011. The value of estuarine and coastal ecosystem services. Ecological Monographs, 81(2), 169-193.

Barreiro, M., 2010. Influence of ENSO and the South Atlantic Ocean on climate predictability over Southeastern South America. Clim. Dyn., 35(7-8), 1493-1508.

Berbery, E.H., Doyle, M. and Barros, V., 2006. Regional precipitation trends. In: Barros, V., Clarke, R.Dias, P.S. (Eds.), Climate change in the La Plata Basin.

Bischoff, S.A., García, N.O., Vargas, W.M., Jones, P.D. and Conway, D., 2000. Climatic Variability and Uruguay River Flows. Water International, 25(3), 446-456.

Bonachea, J., Bruschi, V.M., Hurtado, M.A., Forte, L.M., da Silva, M., Etcheverry, R., Cavallotto, J., Dantas, M.F., Pejon, O.J., Zuquette, L.V., Bezerra, M.A.d.O., Remondo, J., Rivas, V., Gómez-Arozamena, J., Fernández, G. and Cendrero, A., 2010. Natural and human forcing in recent geomorphic change; case studies in the Rio de la Plata basin. Sci. Tot. Environ., 408(13), 2674-2695.

Bouma, T.J., van Belzen, J., Balke, T., Zhu, Z., Airoldi, L., Blight, A.J., Davies, A.J., Galvan, C., Hawkins, S.J., Hoggart, S.P.G., Lara, J.L., Losada, I.J., Maza, M., Ondiviela, B., Skov, M.W., Strain, E.M., Thompson, R.C., Yang, S., Zanuttigh, B., Zhang, L. and Herman, P.M.J., 2014. Identifying knowledge gaps hampering application of intertidal habitats in coastal protection: Opportunities & steps to take. Coastal Eng., 87, 147-157.

Brockmann, C., Doerffer, R., Sathyendranath, S., Ruddick, K., Brotas, V., Santer, R. and Pinnock, S., 2012. The CoastColour dataset, Geoscience and Remote Sensing Symposium (IGARSS), 2012 IEEE International. IEEE, pp. 2036-2039.

Burchard, H. and Baumert, H., 1998. The Formation of Estuarine Turbidity Maxima Due to Density Effects in the Salt Wedge. A Hydrodynamic Process Study. J. Phys. Oceanogr., 28(2), 309-321.

Burrows, M.T., Harvey, R. and Robb, L., 2008. Wave exposure indices from digital coastlines and the prediction of rocky shore community structure. Marine Ecology Progress Series, 353, 1-12.

Butzeck, C., Eschenbach, A., Gröngröft, A., Hansen, K., Nolte, S. and Jensen, K., 2014. Sediment Deposition and Accretion Rates in Tidal Marshes Are Highly Variable Along Estuarine Salinity and Flooding Gradients. Estuar. Coasts, 38(2), 434-450.

Cahoon, D.R., 2006. A review of major storm impacts on coastal wetland elevations. Estuar. Coasts, 29(6), 889-898.

Callaghan, D.P., Bouma, T.J., Klaassen, P., Van der Wal, D., Stive, M.J.F. and Herman, P.M.J., 2010. Hydrodynamic forcing on salt-marsh development: Distinguishing the relative importance of waves and tidal flows. Estuar. Coast. Shelf Sci., 89(1), 73-88.

Cavallotto, J.L., Violante, R.A. and Parker, G., 2004. Sea-level fluctuations during the last 8600 years in the de la Plata river (Argentina). Quat. Int., 114(1), 155-165.

Chen, S.-L., Zhang, G.-A., Yang, S.-L. and Shi, J.Z., 2006. Temporal variations of fine suspended sediment concentration in the Changjiang River estuary and adjacent coastal waters, China. J. Hydrol., 331(1-2), 137-145.

Church, J.A., Clark, P.U., Cazenave, A., Gregory, J.M., Jevrejeva, S., Levermann, A., Merrifield, M.A., Milne, G.A., Nerem, R.S., Nunn, P.D., Payne, A.J., Pfeffer, W.T., Stammer, D. and Unnikrishnan, A.S., 2013. Sea Level Change. In: Stocker, T.F., Qin, D., Plattner, G.-K., Tignor, M., Allen, S.K., Boschung, J., Nauels, A., Xia, Y., V., B.Midgley, P.M. (Eds.), Climate Change 2013: The

Physical Science Basis. Contribution of Working Group I to the Fifth Assessment Report of the Intergovernmental Panel on Climate Change. Cambridge University Press, , Cambridge, United Kingdom and New York, NY, USA.

Clarke, D.W., Boyle, J.F., Chiverrell, R.C., Lario, J. and Plater, A.J., 2014. A sediment record of barrier estuary behaviour at the mesoscale: Interpreting high-resolution particle size analysis. Geomorphology, 221, 51-68.

Colombo, J.C., Cappelletti, N., Barreda, A., Migoya, M.C. and Skorupka, C.N., 2005. Vertical fluxes and accumulation of PCBs in coastal sediments of the Río de la Plata estuary, Argentina. Chemosphere, 61(9), 1345-1357.

D'Onofrio, E., Oreiro, F. and Fiore, M., 2012. Simplified empirical astronomical tide model - An application for the Río de la Plata estuary. Comput. Geosci., 44, 196-202.

Dalrymple, R.W., Zaitlin, B.A. and Boyd, R., 1992. Estuarine facies models; conceptual basis and stratigraphic implications. J. Sediment. Res., 62(6), 1130-1146.

DeLaune, R.D., Whitcomb, J., Patrick, W.H., Pardue, J. and Pezeshki, S.R., 1989. Accretion and canal impacts in a rapidly subsiding wetland. I.137Cs and 210Pb techniques. Estuaries, 12(4), 247-259.

Depetris, P.J., 2007. The parana river under extreme flooding: a hydrological and hydro-geochemical insight. Interciencia, 32, 656-662.

Depetris, P.J., Kempe, S., Latif, M. and Mook, W.G., 1996. ENSO-controlled flooding in the Parana River (1904-1991). Naturwissenschaften, 83(3), 127-129.

Fagherazzi, S., Kirwan, M.L., Mudd, S.M., Guntenspergen, G.R., Temmerman, S., D'Alpaos, A., van de Koppel, J., Rybczyk, J.M., Reyes, E., Craft, C. and

Clough, J.C.R.G., 2012. Numerical models of salt marsh evolution: Ecological, geomorphic, and climatic factors. Rev. Geophys., 50(1), n/a-n/a.

Fiore, M.M.E., D'Onofrio, E.E., Pousa, J.L., Schnack, E.J. and Bértola, G.R., 2009. Storm surges and coastal impacts at Mar del Plata, Argentina. Cont. Shelf Res., 29(14), 1643-1649.

Fossati, M., Cayocca, F. and Piedra-Cueva, I., 2014. Fine sediment dynamics in the Río de la Plata. Advances in Geosciences, 39(39), 75-80.

Framiñan, M.B. and Brown, O.B., 1996. Study of the Río de la Plata turbidity front, Part 1: spatial and temporal distribution. Cont. Shelf Res., 16(10), 1259-1282.

Framiñan, M.B., Etala, M.P., Acha, E.M., Guerrero, R.A., Lasta, C.A. and Brown, O.B., 1999. Physical Characteristics and Processes of the Río de la Plata Estuary. In: Perillo, G.M.E., Piccolo, M.Pino-Quivira, M. (Eds.), Estuaries of South America. Environmental Science. Springer Berlin Heidelberg, pp. 161-194.

Friedrichs, C.T., Armbrust, B.D. and De Swart, H.E., 1998. Hydrodynamics and equilibrium sediment dynamics of shallow, funnel-shaped tidal estuaries. Physics of estuaries and coastal seas, 315-327.

García-Rodríguez, F., Brugnoli, E., Muniz, P., Venturini, N., Burone, L., Hutton, M., Rodríguez, M., Pita, A., Kandratavicius, N., Pérez, L. and Verocai, J., 2014. Warm-phase ENSO events modulate the continental freshwater input and the trophic state of sediments in a large South American estuary. Marine and Freshwater Research, 65(1), 1-11.

García, N.O. and Vargas, W.M., 1998. The Temporal Climatic Variability in the Río De La Plata Basin Displayed by the River Discharges. Clim. Change, 38(3), 359-379.

Grimm, A.M. and Tedeschi, R.G., 2009. ENSO and Extreme Rainfall Events in South America. J. Clim., 22(7), 1589-1609.

Hill, N.A., Pepper, A.R., Puotinen, M.L., Hughes, M.G., Edgar, G.J., Barrett, N.S., Stuart-Smith, R.D. and Leaper, R., 2010. Quantifying wave exposure in shallow temperate reef systems: applicability of fetch models for predicting algal biodiversity. Marine Ecology Progress Series, 417, 83-95.

Holgate, S.J., Matthews, A., Woodworth, P.L., Rickards, L.J., Tamisiea, M.E., Bradshaw, E., Foden, P.R., Gordon, K.M., Jevrejeva, S. and Pugh, J., 2012. New Data Systems and Products at the Permanent Service for Mean Sea Level. J. Coast. Res., 493-504.

Isla, F.I., Schnack, E.J. and Edgardo, M.L., 2009. The Changing Coastlines of South America, Dev. Earth Surf. Process. Elsevier, pp. 49-73.

Jelgersma, S., Healy, T., Marone, E., Terry Healy, Y.W. and Judy-Ann, H., 2002. Relative sea level changes and some effects on muddy coasts. In: Healy, T., Wang, Y.Healy, J.-A. (Eds.), Muddy Coasts of the World: Processes, Deposits and Function. Proceedings in Marine Science. Elsevier Science, Amsterdam, pp. 83-97.

Kirwan, M.L. and Guntenspergen, G.R., 2010. Influence of tidal range on the stability of coastal marshland. Geophys. Res. Lett., 115(F2), F02009.

Kirwan, M.L., Guntenspergen, G.R., D'Alpaos, A., Morris, J.T., Mudd, S.M. and Temmerman, S., 2010. Limits on the adaptability of coastal marshes to rising sea level. Geophys. Res. Lett., 37(23), L23401.

Kolker, A.S., Goodbred Jr, S.L., Hameed, S. and Cochran, J.K., 2009. High-resolution records of the response of coastal wetland systems to long-term and short-term sea-level variability. Estuar. Coast. Shelf Sci., 84(4), 493-508.

Laborde, J.L. and Nagy, G.J., 1999. Hydrography and sediment transport characteristics of the Río de la Plata: a review, Estuaries of South America. Springer, pp. 133-159.

Marrero, A., Tudurí, A., Pérez, L., Cuña, C., Muniz, P., Lopes Figueira, R., Michaelovitch de Mahiques, M., Alves de Lima Ferreira, P., Pittauerová, D., Hanebuth, T. and García-Rodríguez, F., 2014. Cambio históricos en el aporte terrígeno de la cuenca del Río de la Plata sobre La Plataforma interna Uruguaya, 21.

Mechoso, C.R. and Iribarren, G.P., 1992. Streamflow in Southeastern South America and the Southern Oscillation. J. Clim., 5(12), 1535-1539.

Menéndez, A., Re, M., Sarubbi, A. and García, P., 2009. A Conceptual Model for Sediment Transport in the Inner Plata River. In: Vionnet, C., García, M.H., Latrubesse, E.M.Perillo, G.M.E. (Editors), River, Coastal and Estuarine Morphodynamics. RCEM 2009. CRC Press, Santa Fe, Argentina.

Mianzan, H., Lasta, C., Acha, E., Guerrero, R., Macchi, G. and Bremec, C., 2001. The Río de la Plata Estuary, Argentina-Uruguay. In: Seeliger, U.Kjerfve, B. (Eds.), Coastal Marine Ecosystems of Latin America. Ecological Studies. Springer Berlin Heidelberg, pp. 185-204.

Möller, I., 2006. Quantifying saltmarsh vegetation and its effect on wave height dissipation: Results from a UK East coast saltmarsh. Estuar. Coast. Shelf Sci., 69(3-4), 337-351.

Möller, I., Kudella, M., Rupprecht, F., Spencer, T., Paul, M., van Wesenbeeck, B.K., Wolters, G., Jensen, K., Bouma, T.J., Miranda-Lange, M. and Schimmels, S., 2014. Wave attenuation over coastal salt marshes under storm surge conditions. Nature Geosci, 7(10), 727-731.

Moreira, D., Simionato, C.G., Gohin, F., Cayocca, F. and Luz Clara Tejedor, M., 2013. Suspended matter mean distribution and seasonal cycle in the Río de La Plata estuary and the adjacent shelf from ocean color satellite (MODIS) and in-situ observations. Cont. Shelf Res., 68(0), 51-66.

Morris, J.T., Sundareshwar, P.V., Nietch, C.T., Kjerfve, B. and Cahoon, D.R., 2002. Responses of coastal wetlands to rising sea level. Ecology, 83(10), 2869-2877.

North, E.W., Chao, S.Y., Sanford, L.P. and Hood, R.R., 2004. The influence of wind and river pulses on an estuarine turbidity maximum: Numerical studies and field observations in Chesapeake Bay. Estuaries, 27(1), 132-146.

Oldfield, F. and Appleby, P.G., 1978. Alternative Approach to Pb-210 Based Sediment Dating. Geophys. J. Roy. Astron. Soc., 53(1), 177-177.

Pennington, W., Tutin, T.G., Cambray, R.S. and Fisher, E.M., 1973. Observations on Lake Sediments using Fallout 137Cs as a Tracer. Nature, 242(5396), 324-326.

Piedra-Cueva, I. and Fossati, M.n., 2007. Residual currents and corridor of flow in the Rio de la Plata. Applied Mathematical Modelling, 31(3), 564-577.

PSMSL, 2015. Tide gauge data.

Rahman, R. and Plater, A.J., 2014. Particle-size evidence of estuary evolution: A rapid and diagnostic tool for determining the nature of recent saltmarsh accretion. Geomorphology, 213, 139-152.

Re, M., Menéndez, A.N. and Amsler, M.L., 2009. Metodología a para la generatcíon de series temporals de descarga sólida de los ríos Paraná de Las Palmas y Paraná Guazú. RIOS 2009.

Restrepo, J.D. and Kjerfve, B., 2000. Magdalena river: interannual variability (1975-1995) and revised water discharge and sediment load estimates. J. Hydrol., 235(1-2), 137-149.

Sanchez-Cabeza, J.A. and Ruiz-Fernández, A.C., 2012. 210Pb sediment radiochronology: An integrated formulation and classification of dating models. Geochim. Cosmochim. Acta, 82, 183-200.

Sarubbi, A., Pittau, M.G. and Menéndez, A.N., 2006. Delta del Paraná: avance del frente e incremento areal, Instituto Nacional del Agua, República Argentina, Ezeiza, Argentina.

Schuerch, M., Dolch, T., Reise, K. and Vafeidis, A.T., 2014. Unravelling interactions between salt marsh evolution and sedimentary processes in the Wadden Sea (southeastern North Sea). Prog. Phys. Geog., 38(6), 691-715.

Schuerch, M., Rapaglia, J., Liebetrau, V., Vafeidis, A. and Reise, K., 2012. Salt Marsh Accretion and Storm Tide Variation: an Example from a Barrier Island in the North Sea. Estuar. Coasts, 35(2), 486-500.

Schuerch, M., Vafeidis, A., Slawig, T. and Temmerman, S., 2013. Modeling the influence of changing storm patterns on the ability of a salt marsh to keep pace with sea level rise. Journal of Geophysical Research: Earth Surface, 118(1), 84-96.

Shepard, C.C., Crain, C.M. and Beck, M.W., 2011. The Protective Role of Coastal Marshes: A Systematic Review and Meta-analysis. PLoS ONE, 6(11), e27374.

Ta, T.K.O., Nguyen, V.L., Tateishi, M., Kobayashi, I., Saito, Y. and Nakamura, T., 2002. Sediment facies and Late Holocene progradation of the Mekong River Delta in Bentre Province, southern Vietnam: an example of evolution from a tide-dominated to a tide- and wave-dominated delta. Sediment. Geol., 152(3-4), 313-325.

Tatone, L.M., Bilos, C., Skorupka, C.N. and Colombo, J.C., 2015. Trace metal behavior along fluvio-marine gradients in the Samborombón Bay, outer Río de la Plata estuary, Argentina. Cont. Shelf Res., 96, 27-33.

Temmerman, S., Govers, G., Wartel, S. and Meire, P., 2004. Modelling estuarine variations in tidal marsh sedimentation: response to changing sea level and suspended sediment concentrations. Mar. Geol., 212(1-4), 1-19.

Temmerman, S., Meire, P., Bouma, T., Herman, P., Ysebaert, T. and De Vriend, H., 2013. Ecosystem-based coastal defence in the face of global change. Nature, 504(7478), 79-83.

Tosi, L., Kruse, E.E., Braga, F., Carol, E.S., Carretero, S.C., Pousa, J.L., Rizzetto, F. and Teatini, P., 2013. Hydro-morphologic setting of the Samborombón Bay (Argentina) at the end of the 21st century. Natural Hazards Earth System Sciences, 13(3), 523-534.

Uncles, R.J., 2002. Estuarine Physical Processes Research: Some Recent Studies and Progress. Estuar. Coast. Shelf Sci., 55(6), 829-856.

Uncles, R.J., Stephens, J.A. and Smith, R.E., 2002. The dependence of estuarine turbidity on tidal intrusion length, tidal range and residence time. Cont. Shelf Res., 22(11-13), 1835-1856.

van der Wal, D. and Pye, K., 2004. Patterns, rates and possible causes of saltmarsh erosion in the Greater Thames area (UK). Geomorphology, 61(3-4), 373-391.

Van Rijn, L., 2010. Tidal phenomena in the Scheldt Estuary. Report, Deltares.

Vermeer, M. and Rahmstorf, S., 2009. Global sea level linked to global temperature. Proceedings of the National Academy of Sciences, 106(51), 21527-21532.

Wetzel, A. and Unverricht, D., 2013. A muddy megaturbidite in the deep central South China Sea deposited ~ 350 yrs BP. Mar. Geol., 346, 91-100.

Wolanski, E. and Gibbs, R.J., 1995. Flocculation of Suspended Sediment in the Fly River Estuary, Papua New Guinea. J. Coast. Res., 11(3), 754-762.